Experimental determination of stiffness distributions and mode shapes of wind turbine blades

Larsen, Gunner Chr.; Kretz, A.

Publication date:
1995

Document Version
Publisher's PDF, also known as Version of record

RISØ

Risø-R-773(EN)

Experimental Determination of Stiffness Distributions and Mode Shapes of Wind Turbine Blades

Gunner C. Larsen and Allan Kretz

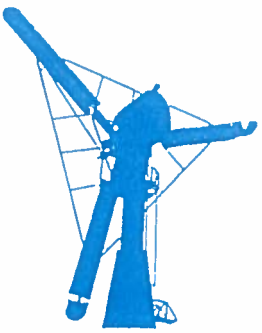

The Test Station for Wind Turbines

Risø National Laboratory, Roskilde, Denmark
March 1995

Experimental Determination of Stiffness Distributions and Mode Shapes of Wind Turbine Blades

Risø-R-773(EN)

Gunner C. Larsen and Allan Kretz

Risø National Laboratory, Roskilde, Denmark
March 1995

Abstract Two non–destructive experimental methods, related to the structural properties of wind turbine blades, have been formulated and applied to two different blades.

The first method deals with determination of the flexural rigidities of wind turbine blades and is based on static deflection measurements. The procedure has been applied to determine distribution of flapwise– and edgewise flexural rigidities of the LM17 m and the LM19 m blade. The findings have been compared to results obtained from cross section calculations, and the overall agreement between measured and calculated flexural rigidities is good, except for the edgewise rigidities related to the LM19 m blade, where some deviations are observed. The reason for this disagreement is believed to be a poor resolution of the curvature in the root part of the blade due to a seemingly hinge like edgewise deformation mechanism here.

The second method deals with the determination of blade mode shapes. The method is founded on an experimental determination of the transfer function relating a dynamic loading with the corresponding acceleration response in a suitable number of points along the structure. The method has succesfully been used to determine the first flapwise and edgewise natural modes of the LM17 m blade, and natural modes of the LM19 m blade related to the first flapwise–, the second flapwise–, and the first edgewise natural frequency.

The development and verification of the present experimental methods are part of the "Concept Testing Program" at the Test Station for Wind Turbines and have been supported by the *Danish Ministry of Energy*, contract no. *ENS–5332/93–001*.

The present report has passed an internal review at The Test Station for Wind Turbines at Risø, performed by:

Troels Friis Pedersen *Flemming Rasmussen*

ISBN 87–550–2015–1
ISSN 0106–2840

Grafisk Service · Risø · 1995

Contents

1 Introduction

Information about the distribution of the *flexural rigidity*, related to the flapwise– and the edgewise principal directions of wind turbine blade cross sections, is essential for aeroelastic simulations of wind turbine structures. These elastic properties are traditionally derived from cross section calculations, in a suitable number of characteristic cross sections, based upon the geometric– and the material design specifications of the blade.

However, due to the complexities in geometry and in the behaviour of the applied composite materials, together with the uncertainties inherent in the blade production process, it is usually desirable to compare the calculated results with experimental data. In addition, the knowledge gained is a prerequisite for validating and improving the analytical methods.

An experimental method, based on static deflection measurements, is described, and the results from an application both to the LM17 m blade and to the LM19 m blade are given and discussed.

The mass distribution is also obtainable from calculations as well as from (non-destructive) experimental tests [1]. As with the distribution of the flexural rigidity, the determination of the mass distribution is also encumbered with uncertainty, although moderate.

A tool, which can be applied to cope with these uncertainties, is an experimental determination of the blade *mode shapes*. These can be obtained with convincing accuracy. By comparing experimentally determined mode shapes with the mode shapes calculated based on the measured mass- and stiffness distributions, these can be modified to approach the correct mode shapes.

A method applicable for an experimental determination of the mode shapes is thus described, and, as with the stiffness distribution, the method has been verified on the LM17 m blade as well as on the LM19 m blade to produce flapwise– and edgewise mode shapes.

2 Flexural rigidity

A procedure for an experimental determination of the flexural rigidity of a wind turbine blade is described. The blade is mounted in a horizontal position with the root part clamped to a rigid test stand. For investigations related to the flapwise flexural rigidity, the tip chord is positioned in a horizontal orientation, whereas for the determination of the edgewise flexural rigidity, the tip chord is positioned in a vertical position.

The blade is then subsequently loaded by a static vertical point force of known size at a known position. The situation is sketched in Fig. 1 below.

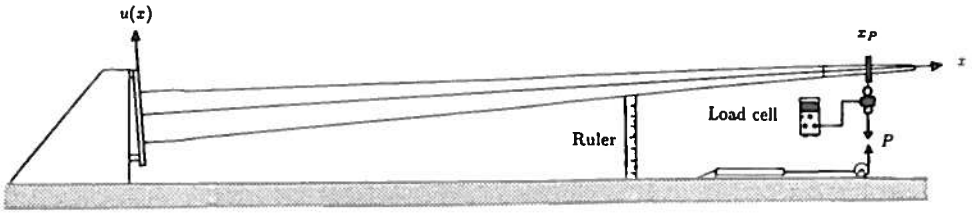

Figure 1. One point loading of a horizontally clamped wind turbine blade.

Denoting by x the coordinate along the undeformed blade axis with zero at the blade flange and increasing values towards the tip, the deflection of the blade axis perpendicular to the x–axis, $u(x)$[1], due to the applied load, P, is recorded in a suitable number of distinct points. The recording is performed by means of a ruler, and the deflection of the blade surface is presumed to equivalate the deflection of the blade axis. The measuring stations are usually equidistant distributed with 0.25 m to 0.50 m between them. Note, that with the setup sketched in Fig. 1, the deflection, originating from the applied point force, is defined negative.

In order to secure sufficient resolution of the deflection in all the selected points on the blade, and at the same time to respect the limited load carrying capacity of the blade in the tip region, it may be necessary to apply external point forces at a number of different points of attack. Usually, a large vertical point force is applied at a position in the vicinity of the middle of the blade to account for the deflection in the root region of the blade, whereas a moderate vertical point force is applied near the tip of the blade in order to account for the deflection of the tip region.

Denoting by x_P the point of attack of the vertical force, the moment, arising from the external loading at the position x, $M_E(x)$[2], is expressed by

$$M_E(x) = P(x_P - x) \qquad \text{for } x \leq x_P \,. \tag{2.1}$$

The corresponding moment, made up by the internal elastic forces, $M_I(x)$, is expressed by[3]

$$M_I(x) = EI(x)\frac{\partial^2 u(x)}{\partial x^2} \qquad \text{for } x \leq x_P \,, \tag{2.2}$$

where $EI(x)$ is the flexural rigidity of the blade cross section defined by x.

[1] As indicated, the blade deflection is independent of time as only static loading is considered.
[2] The moment is independent of time as only static loading is considered.
[3] Assuming small deflections and disregarding the effect of shear forces in the beam model.

Having determined the deflection $u(x)$, the flexural rigidity is thus obtainable, for cross sections satisfying $x \leq x_P$, from the static equilibrium condition. Equalizing the expressions (2.1) and (2.2), we derive at

$$EI(x) = \frac{P(x_P - x)}{\frac{\partial^2 u(x)}{\partial x^2}} \qquad \text{for } x \leq x_P \ . \tag{2.3}$$

It turns out that the determination of the second derivative of a measured deflection curve, with its inherent measuring errors, is a highly delicate process. Therefore, the measured deflection field has to be smoothed by a suitable fitting function. This fitting function must possess the potential to generate the shape of a typical distribution of the flexural rigidity related to a wind turbine blade. In the present investigations, the measured values have been approximated by a fitting function of the form

$$f(x; a_0, ..., a_N) = \exp(\sum_{i=0}^{N} a_i x^i) \qquad \text{for } x \leq x_P \ , \tag{2.4}$$

where $a_0, ..., a_N$ denote the adjustable parameters of the fitting function. The maximum likelihood estimates of these, $a_0^*, ..., a_N^*$, are determined by use of the traditional least square technique. Thus, it is implicitly assumed that the measuring errors are independent Gaussian with identical variance at each of the measuring points [1]. As the measured deflection curve usually is determined by means of an ordinary ruler, this seems to be a reasonable assumption.

The degree of the polynomial in the expression for the fit will depend on the particular situation, as the highest degree, for which the second derivative of the resulting fitted function does not display an oscillating behaviour, has been applied. Having fitted a function $f(x; a_0^*, ..., a_N^*)$ to the measured deflection curve, the flexural rigidity is readily obtained from

$$EI(x) = \frac{P(x_P - x)}{\frac{\partial^2 f(x; a_0^*, ..., a_N^*)}{\partial x^2}} \qquad \text{for } x \leq x_P \ . \tag{2.5}$$

In case $f(x; a_0^*, ..., a_N^*)$ represent the "true" deflection curve, expression (2.5) will be a very good estimate to the "true" flexural rigidity. This is because only the uncertainty originating from the determination of the external moment can make the determined flexural rigidity to deviate from the "true" flexural rigidity, and because the external applied moment is easily determined with an uncertainty less than 1 %. However, the expression $f(x; a_0^*, ..., a_N^*)$ will usually be exposed to some scatter, partly due to the statistical uncertainties inherent in the deflection measurements, and partly due to the assumption concerning the form[4] of the fitted deflection as expressed in equation (2.4).

The scatter in $f(x; a_0^*, ..., a_N^*)$ will introduce scatter in the second derivative of the maximum likelihood fit $f''(x_P; a_0^*, ..., a_N^*)$. In order to eliminate some of the scatter in the second derivative of the fitted function, a series of tests, with different size of the applied vertical forces P_i, are performed for each point of attack. Suppose, that J tests are performed with the point of attack defined by $x = x_P$. The normalized curvature, expressed by

$$\bar{\kappa}(x) = \frac{\frac{\partial^2 f(x; a_0^*, ..., a_N^*)}{\partial x^2}}{P(x_P - x)} \qquad \text{for } x \leq x_P \ , \tag{2.6}$$

[4]Note, that most of the boundary conditions are violated with the present choice of $f(x; a_0^*, ..., a_N^*)$, as neither of $f(0; a_0^*, ..., a_N^*) = 0$, $f'(0; a_0^*, ..., a_N^*) = 0$, or $f''(x_P; a_0^*, ..., a_N^*) = 0$ is forced to be satisfied. The prime in the expressions denote partial derivation with respect to the coordinate x. However, it appears from expression (2.5) that the boundary condition related to the shear force, $P = -\frac{d}{dx} M_E(x)$, is identical satisfied.

should, for ideal conditions, be an invariant for all tests. However, due to the scatter (primarily) in the determined values for the second derivative of the fitted function, the realizations $\bar{\kappa}_i(x)$, $i = 1, ..., J$ are observed. As a best estimate to the "true" value of $\kappa(x)$, the mean value, expressed by

$$\bar{\bar{\kappa}}(x) = \frac{1}{J}\sum_{i=1}^{J}\bar{\kappa}_i(x) \qquad \text{for } x \leq x_P\,, \tag{2.7}$$

is applied, thus finally expressing the flexural rigidity as

$$\overline{EI}(x) = \frac{1}{\bar{\bar{\kappa}}(x)} \qquad \text{for } x \leq x_P\,. \tag{2.8}$$

2.1 Flapwise stiffness of the LM17 m blade

The method described in the previous section has been applied to determine the flapwise flexural rigidity of the LM17 m blade. Two series of load cases have been performed - the first with the point of attack defined by $x_P = 11.47\ m$, and the second with the point of attack specified as $x_P = 14.90\ m$. Both test series consisted of three load cases. In the first test series, the point forces were assigned the values $P_1 = 13748\ N$, $P_2 = 20622\ N$, and $P_3 = 26219\ N$. In the second test series, the point forces were given the values $P_1 = 2386\ N$, $P_2 = 4959\ N$, and $P_3 = 6540\ N$. The measured deflection data are generally of good quality, and for both load series these are presented in Appendix A.

For each of the experiments, a deflection curve was fitted to the measured data according to expression (2.4) with the polynomial degree $N = 3$. The results are illustrated in Fig. 2 and in Fig. 3, where representative measured deflection data have been plotted together with the corresponding fitted deflection.

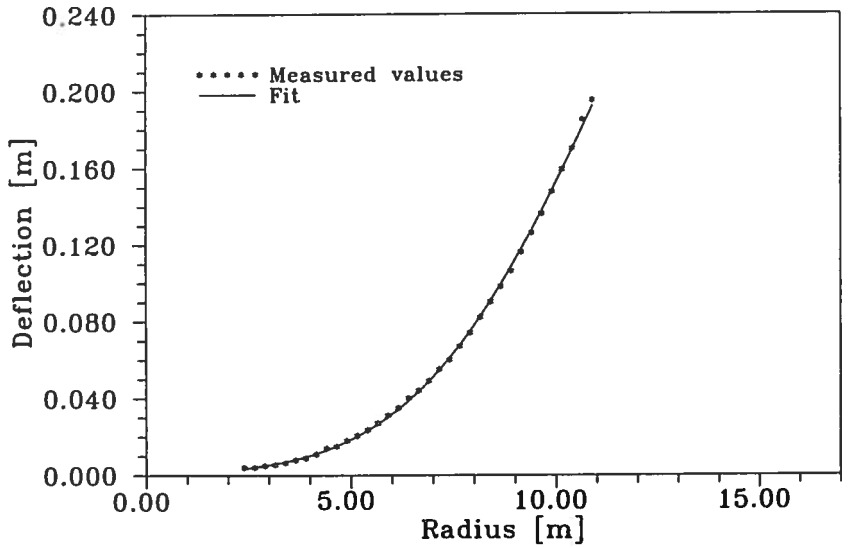

Figure 2. Measured and fitted deflection data related to the load case defined by $P_3 = 26219\ N$ and $x_P = 11.47\ m$.

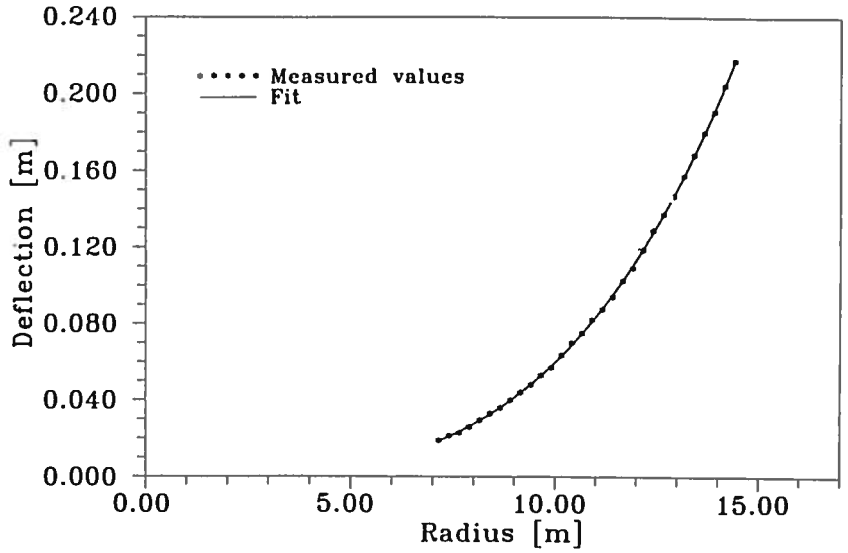

Figure 3. Measured and fitted deflection data related to the load case defined by $P_3 = 6540\ N$ *and* $x_P = 14.90\ m$.

As seen, the general agreement between the measured and fitted deflections is good. Although the boundary conditions by no means are secured by a fit of the specified type, an inspection shows that they are reasonable well satisfied. By extrapolating the fit shown in Fig. 2, it appears that the deflection as well as the gradient of the deflection at the clamped point is close to zero. Moreover, the second derivative of the fitted deflection is close to zero at the point of attack, thus securing a value of the imposed moment at this point close to zero. This is illustrated in Fig. 4.

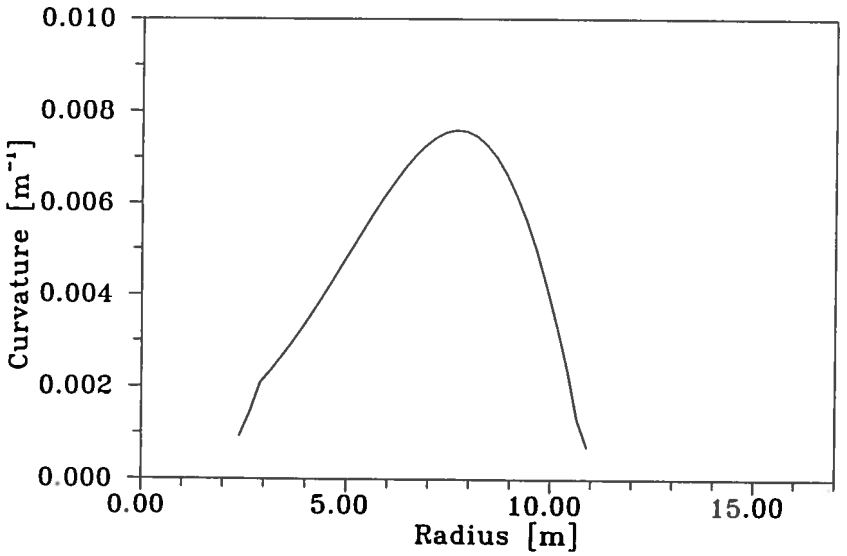

Figure 4. Curvature of the fitted deflection data related to the load case defined by $P_3 = 26219\ N$ *and* $x_P = 11.47\ m$.

The distribution of the flexural rigidity, as obtained from expression (2.5), is displayed in Fig. 5 for all the load cases contained in the present two test series.

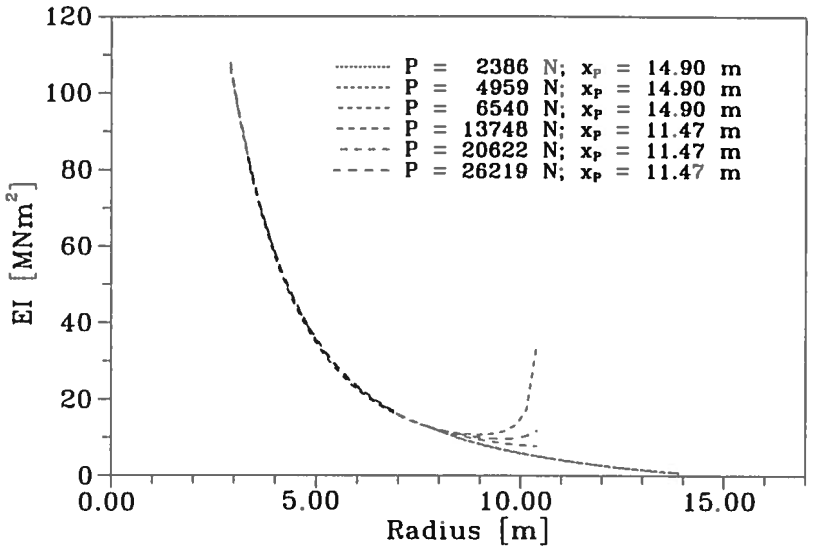

Figure 5. Flexural rigidities determined based on all the load cases.

Due to the dominating stiffness in the part of the blade close to the root flange compared to the stiffness in other parts of the blade, it is not possible to resolve the stiffness in that part based on the selected load cases. However, it is clearly not a principal defect with the method. As the most interesting part of the blade, in relation to the dynamic behaviour, seems to be resolved by the selected load cases, it was decided not to extend the measuring programme to capture the flexural rigidity in the region very close to the root flange.

As seen from Fig. 5, the two categories of curves, corresponding to the two test series, seems to meet "smooth" in the vicinity of $x = 7.65\ m$, and moreover each of the curve categories display very limited mutual scatter. In Fig. 6, the final flapwise flexural rigidity has been estimated by unifying the mean of the two test series, as determined from expression (2.8), at the point $x = 7.65\ m$.

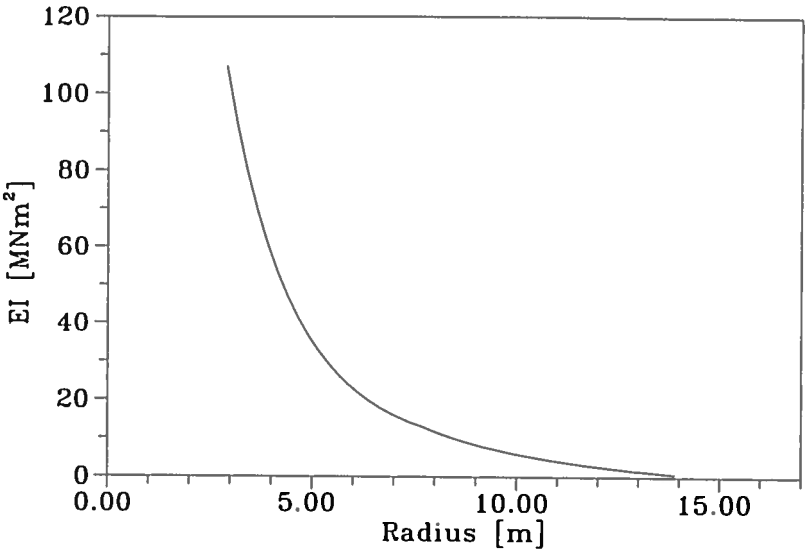

Figure 6. Resulting flapwise flexural rigidity.

2.2 Edgewise stiffness of the LM17 m blade

The edgewise flexural rigidity of the LM17 m blade is now addressed. As with the flapwise stiffness, two series of load cases have been considered - the first related to the point of attack defined by $x_P = 10.00\ m$, and the second related to the point of attack specified as $x_P = 16.65\ m$. Again, both test series consisted of three load cases. In the first test series, the point forces were assigned the values $P_1 = 13748\ N$, $P_2 = 15417\ N$, and $P_3 = 20818\ N$. In the second test series, the point forces $P_1 = 2386\ N$, $P_2 = 3938\ N$, and $P_3 = 5234\ N$ were applied. The measured deflection data are for both load series listed in Appendix B.

A deflection curve has been fitted to the measured data according to expression (2.4) for each of the load situations. For the data related to the first test series, fits defined by $N = 1$ were applied, whereas fits with the polynomial degree $N = 2$ were used to approximate the data originating from the second test series. The results are illustrated in Fig. 7 and in Fig. 8, where representative measured deflection data have been plotted together with their corresponding fitted deflection.

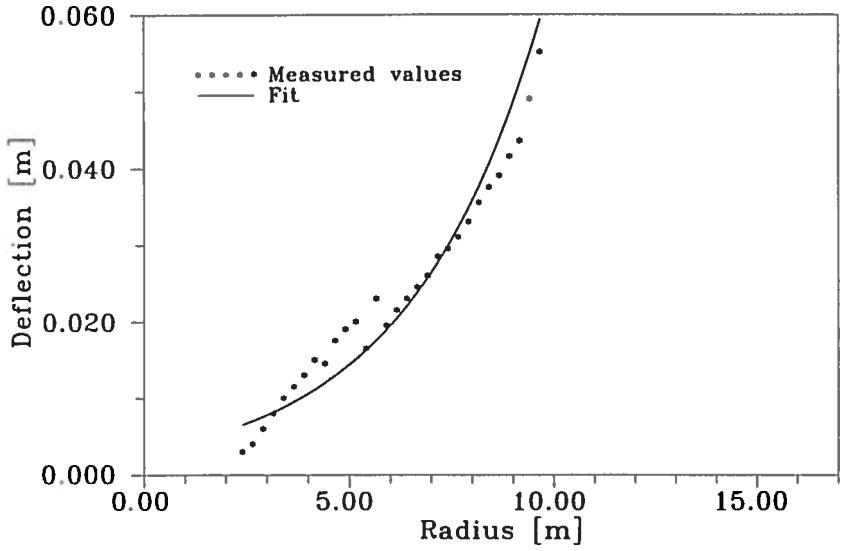

Figure 7. Measured and fitted deflection data related to the load case defined by $P_3 = 20818\ N$ *and* $x_P = 10.00\ m$.

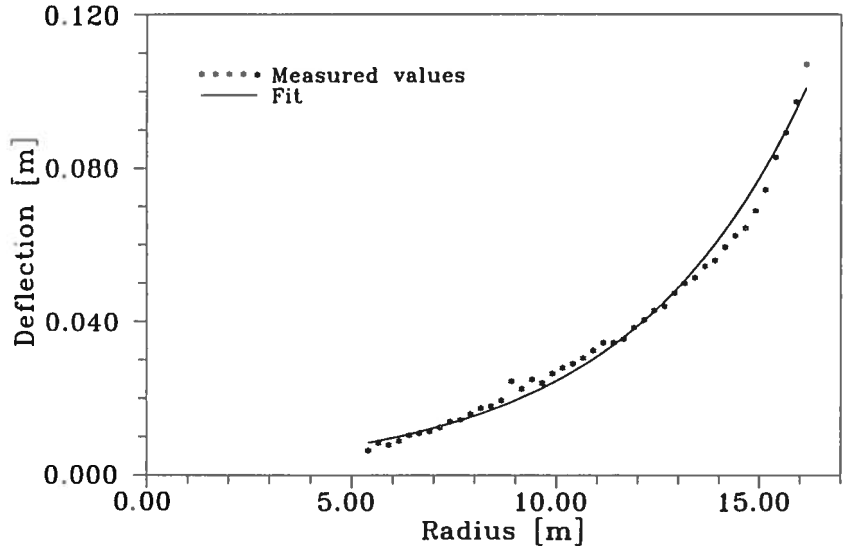

Figure 8. Measured and fitted deflection data related to the load case defined by $P_3 = 5234\ N$ *and* $x_P = 16.65\ m$.

As seen, some deviation between the fits and the measurements has been encountered, especially for the first load series[5]. The second test series displays generally good agreement between the measured and fitted deflections, however, the hinge like mechanism, at the position where the aerodynamic tip guide is the only load carrying component, is not resolved.

The resulting distribution of the flexural rigidity, as obtained from expression (2.5), is presented in Fig. 9 for all the load cases contained in the two test series.

[5]This is in accordance with the low polynomial degree of the fit obtained here.

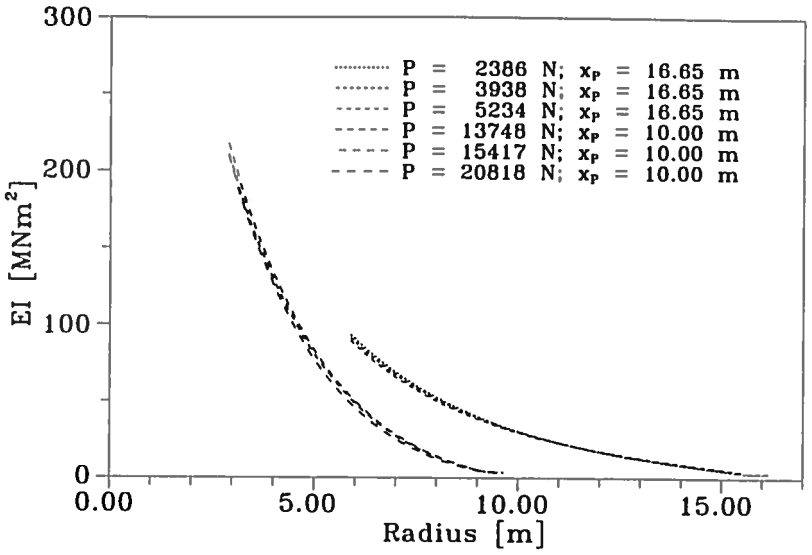

Figure 9. Flexural rigidities determined based on all the load cases.

The mutual agreement between load situations corresponding to the same point of attack is good, but a considerable jump in level is observed between the two curve categories. This discrepancy is believed, primarily, to originate from the essential deviations between fits and measurements related to the first test series. The considerable deviations seriously affect the determination of the second derivative, which is the base for the determination of the flexural rigidity. As a conclusion, only the distributions of the flexural rigidity related to the second test series are considered reliable. The final edgewise flexural rigidity, defined as the mean, in the sense expressed by (2.8), of the contributing load situations related only to the second test series, is shown in Fig. 10.

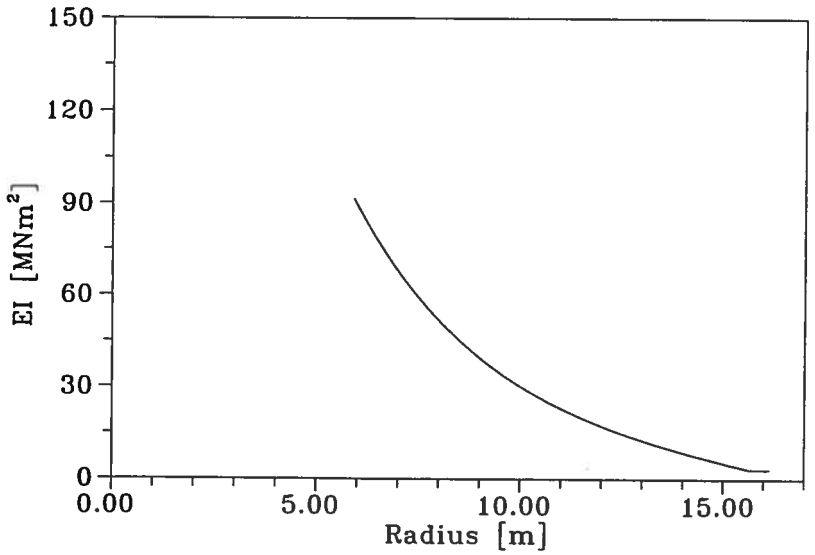

Figure 10. Resulting edgewise flexural rigidity.

2.3 Flapwise stiffness of the LM19 m blade

The flapwise flexural rigidity of the LM19 m blade is considered in this section. The procedure is completely identical to the procedure applied for the determination of the flapwise flexural rigidity related to the LM17 m blade.

Two series of load cases, with points of attack specified by $x_P = 13.07\ m$ and $x_P = 18.50\ m$, respectively, have been performed. Both test series consisted of three load cases, and the first test series embraced the load situations defined by $P_1 = 9820\ N$, $P_2 = 16989\ N$, and $P_3 = 23470\ N$, whereas in the second test series, the point forces $P_1 = 1954\ N$, $P_2 = 3064\ N$, and $P_3 = 4939\ N$ were applied. The measured deflection curves are generally of good quality, and the specific measuring results from both load series are given in Appendix C.

The fits to the measured deflections have been performed with a variety of different polynomial degrees applied in expression (2.4). As for the first load series, the P_3–load situation was fitted by applying $N = 6$, whereas in the remaining two load situations the value $N = 3$ was used. In the second load series, the P_1–, P_2–, and P_3 load situations were fitted by applying $N = 3$, $N = 5$, and $P = 7$, respectively. Two representative fits are shown in Fig. 11 and in Fig. 12, together with the corresponding measured deflection data, and the agreement is most satisfactory.

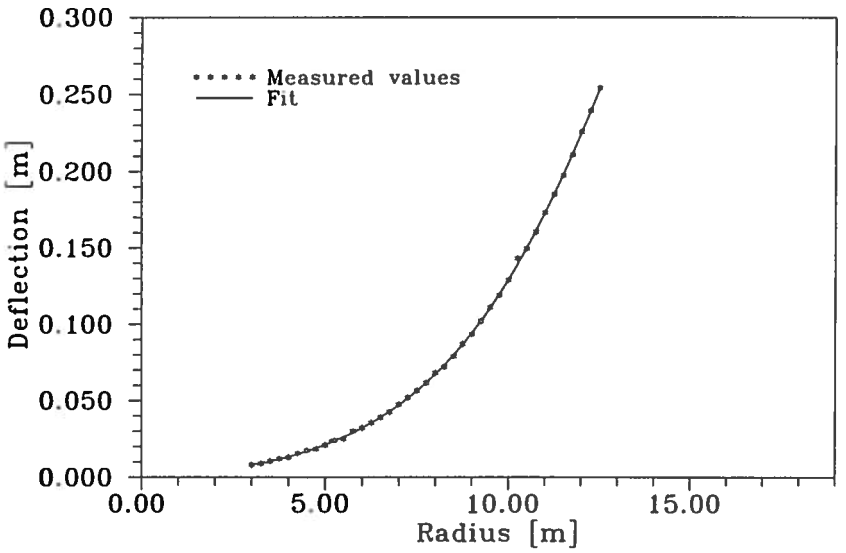

Figure 11. Measured and fitted deflection data related to the load case defined by $P_3 = 23470\ N$ *and* $x_P = 13.07\ m$.

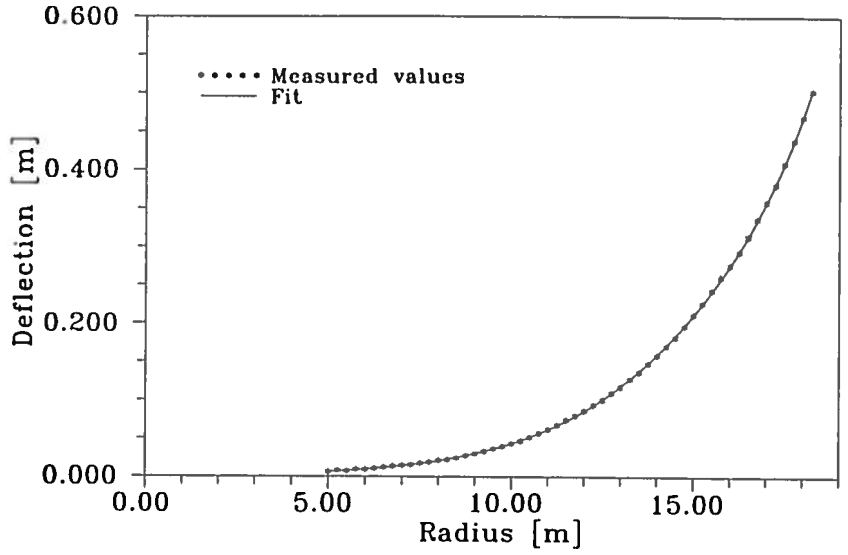

Figure 12. Measured and fitted deflection data related to the load case defined by $P_3 = 4939\ N$ *and* $x_P = 18.50\ m$.

The distribution of the flexural rigidity, as obtained from expression (2.5), is shown in Fig. 13 for all the load cases contained in the two test series.

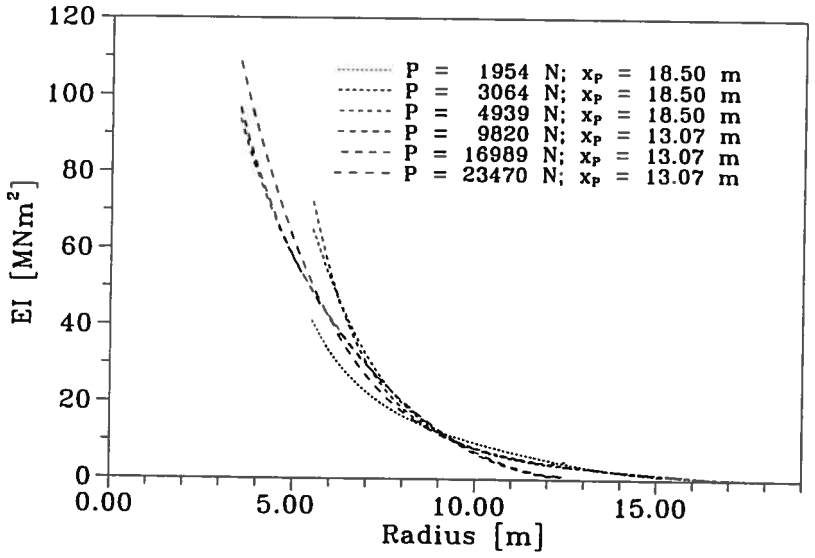

Figure 13. Flexural rigidities determined based on all the load cases.

As it appears from Fig. 13, the two categories of curves, corresponding to the two test series, nearly coincide in the vicinity of the terminal point $x = 9\ m$, and furthermore limited mutual scatter is observed among curves belonging to the same category. In Fig. 14, the final flapwise flexural rigidity has been estimated by applying the averaging procedure, defined by expression (2.8), for each of the two test series, and then subsequently assemble these curves at $x = 9\ m$.

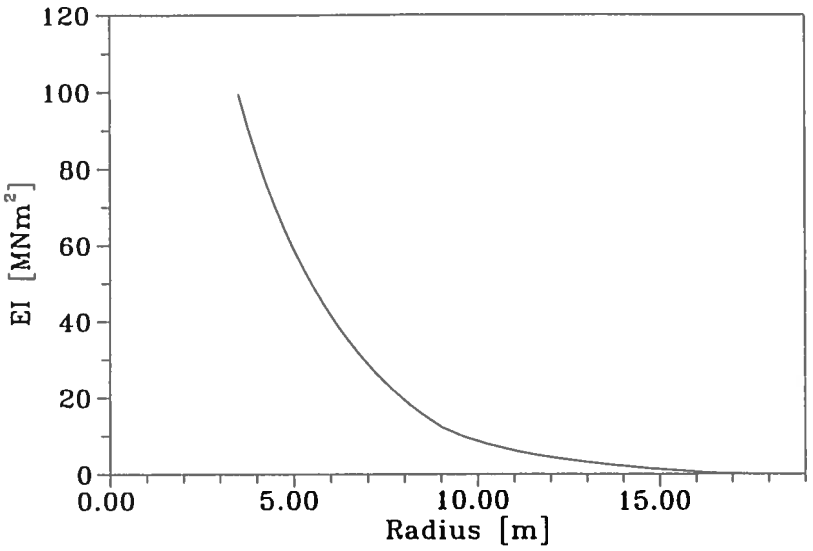

Figure 14. Resulting flapwise flexural rigidity.

2.4 Edgewise stiffness of the LM19 m blade

An attempt to determine the edgewise flexural rigidity for the LM19 m blade has been done using two test series with the points of attack specified by $x_P = 13.07\ m$ and $x_P = 18.50\ m$, respectively. In the first test series, related to the point of attack defined by $x_P = 13.07\ m$, the point forces $P_1 = 7070\ N$, $P_2 = 14926\ N$, $P_3 = 21506\ N$, and $P_4 = 30737\ N$ were applied, whereas the second test series was constituted by the forces $P_1 = 2966\ N$, $P_2 = 3948\ N$, and $P_3 = 5440\ N$. The measured deflection curves are generally of good quality, and the measured deflection data for both load series can be found in Appendix D. However, for the test series related to the point of attack specified by $x_P = 13.07\ m$, the curvature of the measured deflection curve is diminutive as illustrated in Fig. 15 for the load situation defined by $P_3 = 30737\ N$.

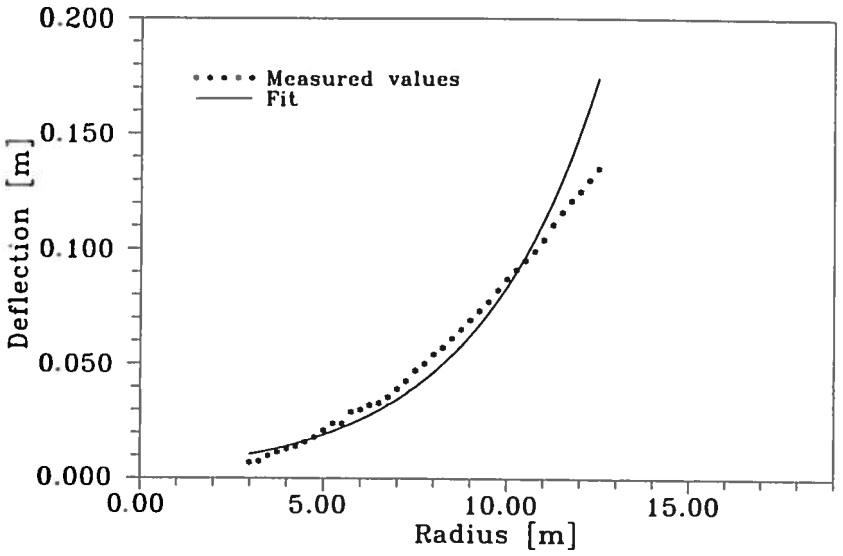

Figure 15. Measured and fitted deflection data related to the load case defined by $P_3 = 30737\ N$ *and* $x_P = 13.07\ m$.

The small curvature is considered to originate from a deformation mechanism, where the root part close to the flange to some degree acts as a hinge, due to a relative substantial larger edgewise stiffness in the region of the blade where the chord lengths are considerable. The small values of the curvature result in large uncertainties when based on a fit of the type defined by expression (2.4). In the present case, the highest possible[6] degree of the polynomial, in the expression for the fitted curves, was $N = 1$. The resulting fits display in general too large curvatures, especially in the "outer" region, as illustrated for a representative example in Fig. 15. As a consequence, the distribution of the flexural rigidities is expected to display too small values in the same region. This is also reflected in the results presented in Fig. 17.

For the second test series, the fits to the measured deflections are performed with $N = 2$. In general, good agreement is encountered between fits and measurements. However, the crease on the measured curve, related to the aerodynamic tip brake structure, is not resolved. As an example, the measured and fitted deflections, originating from applying the force $P_3 = 5440\ N$ at $x_P = 18.50\ m$, are shown in Fig. 16.

[6] In the sense described in section 2.

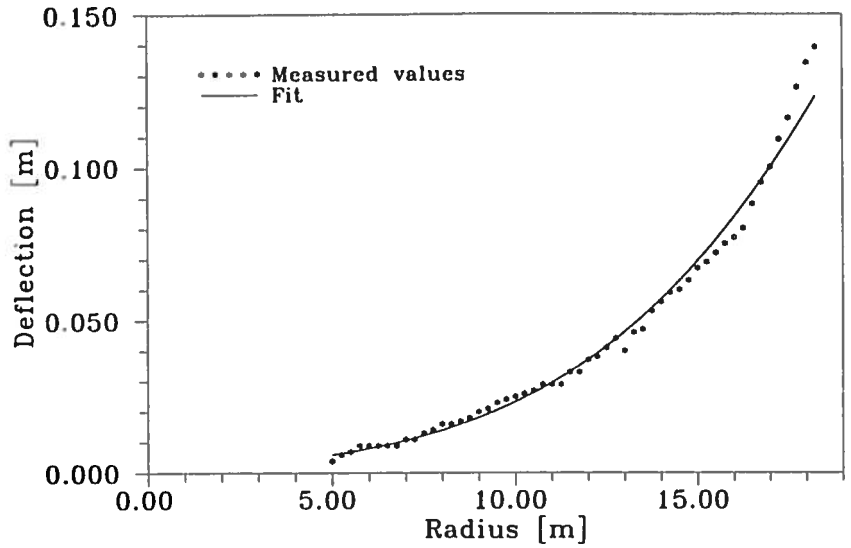

Figure 16. Measured and fitted deflection data related to the load case defined by $P_3 = 5440\ N$ *and* $x_P = 18.50\ m$.

The distribution of the edgewise flexural rigidity, as determined from expression (2.5), is shown in Fig. 17 for all the load cases contained in the two test series.

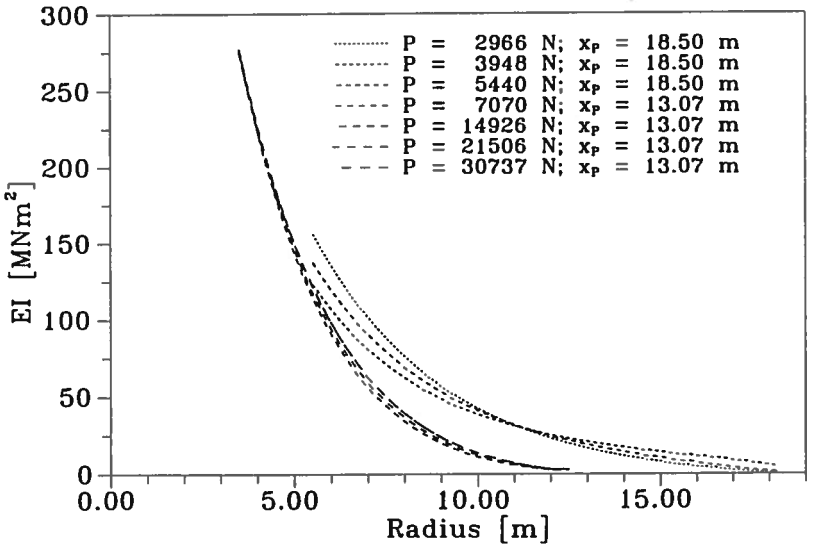

Figure 17. Flexural rigidities determined based on all the load cases.

As appears, the mutual agreement among load situations related to the same test series are good. However, as expected, considerable deviation in levels between the two test series in the "overlap region" is displayed. Based on the considerations concerning the fits to the measured data from the first test series, only the analysis related to the second test series is considered reliable.

The resulting edgewise flexural rigidity is thus determined as the mean of the second test series derived in accordance with expression (2.8). The result is shown in Fig. 18.

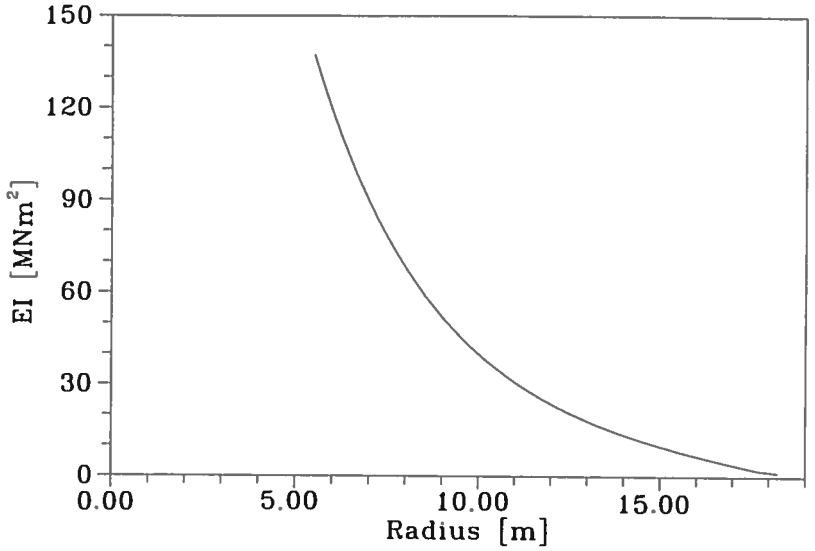

Figure 18. Resulting edgewise flexural rigidity.

2.5 Evaluation of results

The resulting measured flapwise and edgewise flexural rigidities, obtained in the previous sections, have been compared to results obtained from cross section calculations performed by LM Glasfiber as a part of the blade approval procedure. The results are displayed in Fig. 19, Fig. 20, Fig. 21, and Fig. 22.

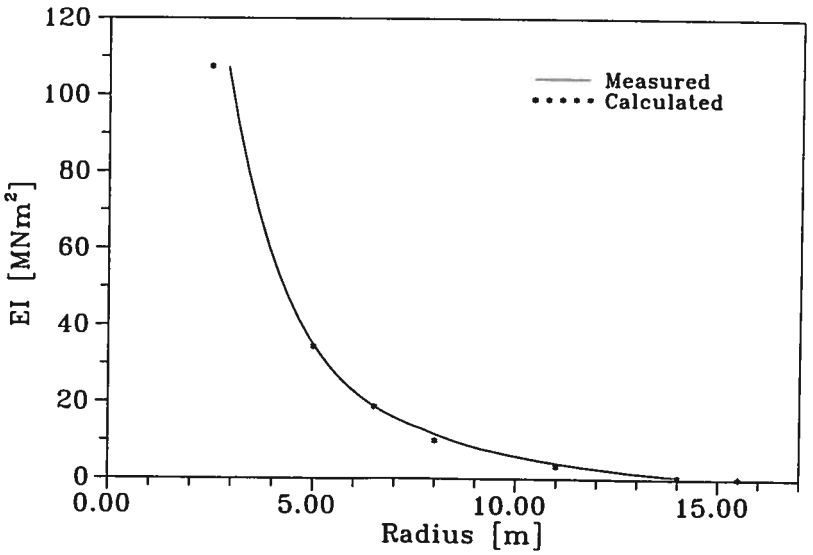

Figure 19. Measured and calculated flapwise flexural rigidities of the LM17 m blade.

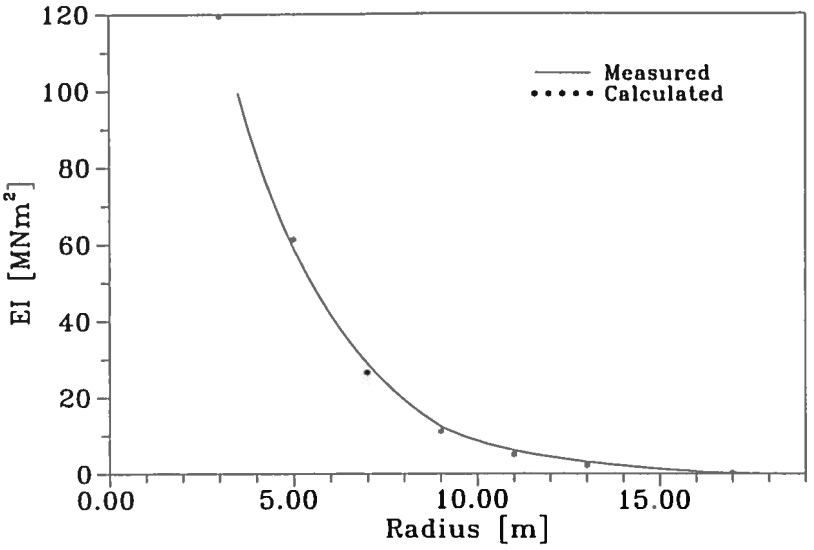

Figure 20. Measured and calculated flapwise flexural rigidities of the LM19 m blade.

As appears, the overall agreement between measured and calculated flapwise flexural rigidities is good, which indicate that the measuring procedure is not significantly distorted by effects as local buckling of the surface, creep in the material, and coupling between bending and torsion in the pretwisted blade. However, the resolution of the deformation in the blade part close to the root is not sufficient to enable a determination of the flexural rigidity here, but this could be compensated for by increasing the loading[7].

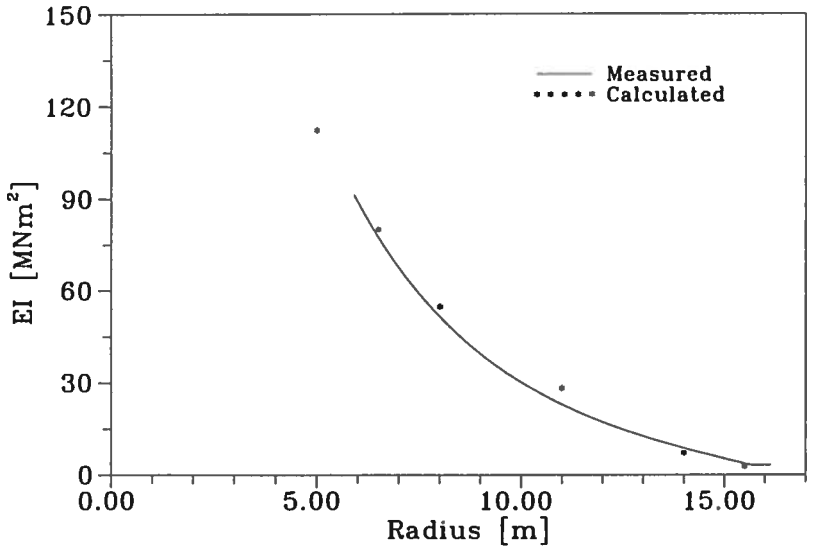

Figure 21. Measured and calculated edgewise flexural rigidities of the LM17 m blade.

[7]In case an increase in the size of the (point) loading conflict with the load carrying capasity of the blade surface, the method is easily extended to a situation where two or more point forces are applied simultaneously.

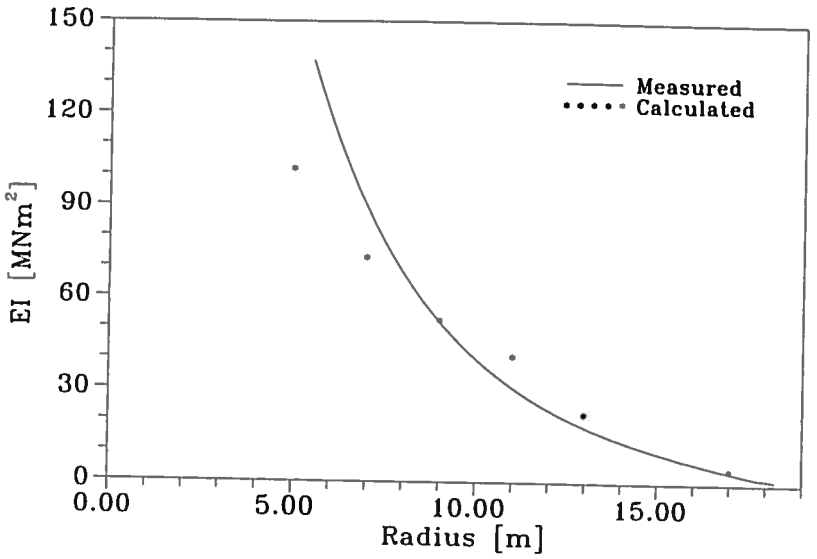

Figure 22. Measured and calculated edgewise flexural rigidities of the LM19 m blade.

The agreement between measured and calculated edgewise rigidities of the LM17 m blade is satisfactory. However, the insufficient resolution in the root part is even more pronounced here than in the flap–situation as commented on previously. Conserning the edgewise rigidities of the LM19 m blade some deviation is observed, and the poor resolution of the curvature in the root part is difficult to circumvent due to the seemingly hinge like deformation mechanism here.

3 Mode shapes

The present section concerns an investigation of the *dynamic properties* of wind turbine blades. The method, to be presented, relies heavily on a *presumption* of linearity[8] of the test structure, in the sense that the *principle of superposition* applies. In practice, real structures are seldom completely linear although, for practical purposes, many will closely approximate this state, at least for moderate deflections. Moreover, the mass of the transducer is *assumed negligible*, relative to the mass of the vibrating part of the structure, in the sense that the presence of the transducer do not affect the response of the structure.

The vibration modes of a structure are classified into the categories *normal modes* and *complex modes*, according to whether all parts of the structure are moving either in phase or 180 degrees out of phase with each other, or, alternatively, any phase relationship, between different parts of the structure, is revealed. The above classification is closely related to the damping characteristics of the structure, which result from a combination of contributions from viscos–, hysteretic–, columb–, and aerodynamic damping. However, in many practical situations the damping is small, and simplifying assumptions can be made.

In the present investigation *proportional damping* is presumed, for which the damping is proportional to the mass and/or the stiffness properties. Under these circumstances normal modes prevail, which is illustrated in the following.

Let the wind turbine blade be approximated by a simple *linear elastic*[9] beam with the torsional degree of freedom neglected such that no *structural coupling* between the principal flap– and edgewise motion exists. The deflections, $u(x,t)$, of the structure, in the flapwise and edgewise principal directions, are then expressed in terms of uncoupled differential equations of the form:

$$\frac{\partial^2}{\partial x^2}\left[E(x)I(x)\frac{\partial^2 u(x,t)}{\partial x^2} + c_s(x)I(x)\frac{\partial^3 u(x,t)}{\partial x^2 \partial t}\right] + m(x)\frac{\partial^2 u(x,t)}{\partial t^2} + c(x)\frac{\partial u(x,t)}{\partial t} = p(x,t)\,, \tag{3.1}$$

where the description is performed in a Cartesian blade coordinate system with the x–axis directed along the undeformed blade axis and $x = 0$ corresponding to the blade flange position. $u(x,t)$ is directed in the principal flapwise or in the principal edgewise direction, depending on the situation under consideration, and the time is denoted by t. The structural quantities $E(x)I(x)$, and $I(x)$ are the flexural rigidity and the moment of inertia referring to the relevant deflection. The mass per unit length is denoted by $m(x)$, $c_s(x)$ is the strain damping, and $c(x)$ the velocity damping. The applied external force per unit length, directed along the direction of the deflection, is $p(x,t)$.

[8] A quantitative test on linearity can be performed, based on a measured complex frequency response function (resulting from a sinusoidal excitation), by applying the Hilbert Transform as described in [2, p.151]. The procedure requires a computation based on the measured frequency response function. In the present experimental setup, the frequency response function was determined directly by use of an analyzer, and the functional values was not made accessible for succeeding analysis. Therefore, an explicit test on linearity has not been performed. However, based on experience with aeroelastic codes, which usually also relies on a linearity assumption, the present blades do, in the authors opinion, exhibit a linear behaviour.

[9] This implies that only small deflections can be dealt with.

Let us take advantage of the modal decomposition technique, and expand the deflection in terms of the normal vibration modes as

$$u(x,t) \equiv \sum_{i=1}^{\infty} \varphi_i(x) q_i(t) \ , \tag{3.2}$$

where $q_i(t)$ are the modal amplitude functions[10], and $\varphi_i(x)$ are the normal vibration modes, corresponding to the free undamped oscillations, determined by

$$\frac{\partial^2}{\partial x^2}\left[E(x)I(x)\frac{\partial^2 \varphi_i(x)}{\partial x^2}\right] q_i(t) + m(x)\varphi_i(x)\ddot{q}_i(t) = 0 \ . \tag{3.3}$$

The symbol $\ddot{(\cdot)}$ indicates differentiation twice with respect to time. Expressing the assumption of orthogonal damping as

$$c_s(x) \equiv \beta E(x) \ , \tag{3.4}$$

and

$$c(x) \equiv \varepsilon m(x) \ , \tag{3.5}$$

where β and ε are constants, the following equations [4] are finally obtained for the modal amplitude functions:

$$\ddot{q}_i(t) + \left(\varepsilon + \beta\omega_i^2\right)\dot{q}_i(t) + \omega_i^2 q_i(t) = \frac{1}{m_i}\int_0^L \varphi_i(x) p(x,t) dx \ , \tag{3.6}$$

with L denoting the length of the blade, and the *generalized mass*, corresponding to the i'th vibration mode, defined according to

$$m_i = \int_0^L \varphi_i^2(x) m(x) dx \ . \tag{3.7}$$

The term $c_{st}^i = (\varepsilon + \beta\omega_i^2)$ taken together is denoted the *structural damping* related to the i'th mode, often expressed as

$$(\varepsilon + \beta\omega_i^2) = 2\omega_i \xi_{si}, \tag{3.8}$$

where ξ_{si} is the *structural damping ratio* related to the i'th vibration mode. As ε and β are constants, it is seen that the structural damping ratio varies with the vibration mode.

In the present test situation, the structure will be exposed to a harmonicly varying point force with amplitude $P(x_P)$ at the position x_P and with the frequency equal to ω_0. The load term is thus expressed as

$$p(x,t) = P(x_P)\delta(x - x_P)e^{i\omega_0 t} \ , \tag{3.9}$$

where $\delta(\cdot)$ is the Dirac function. By introducing expressions (3.8) and (3.9) into (3.6), we obtain the following equations for the modal amplitude functions related to the harmonic excitation

$$\ddot{q}_i(t) + 2\omega_i\xi_{si}\dot{q}_i(t) + \omega_i^2 q_i(t) = \frac{1}{m_i}\varphi_i(x_P)P(x_P)e^{i\omega_0 t} \ . \tag{3.10}$$

The frequency domain formulation, corresponding to the above time domain for-

[10] In the modal formulation, the $q_i(t)$-quantities is often referred to as *generalized coordinates*.

mulation of the deterministic response, is achieved by taking the Fourier transform on both sides of relation (3.10). Thus, the following expressions emerge

$$-\omega^2\tilde{q}_i(\omega) + 2j\omega\omega_i\xi_{si}\tilde{q}_i(\omega) + \omega_i^2\tilde{q}_i(\omega) = \frac{1}{m_i}\varphi_i(x_P)P(x_P)\delta(\omega-\omega_0) \ , \qquad (3.11)$$

where j denotes the imaginary unit, and the complex modal amplitudes, $\tilde{q}_i(\omega)$, are given by

$$\tilde{q}_i(\omega) = \frac{1}{2\pi}\int_{-\infty}^{\infty} q_i(t)e^{-i\omega t}dt \ . \qquad (3.12)$$

In arriving at relation (3.11), it has been utilized that the coefficients to the modal amplitude function and its derivatives in (3.10) are time independent. Complex frequency response functions, $H_i(\omega)$, are subsequently introduced as

$$H_i(\omega) \equiv m_i^{-1}\left[-\omega^2 + 2j\omega\omega_i\xi_{si} + \omega_i^2\right]^{-1} \ , \qquad (3.13)$$

and the generalized coordinates expressed in the frequency domain, and related to the present vibration problem, are then obtained from

$$\tilde{q}_i(\omega) = H_i(\omega)\varphi_i(x_P)P(x_P)\delta(\omega-\omega_0) \ . \qquad (3.14)$$

In the frequency domain, the contribution to the total deflection, originating from the i'th mode, $\tilde{u}_i(x,\omega)$, is consequently expressed as

$$\tilde{u}_i(x,\omega) = \tilde{q}_i(\omega)\varphi_i(x) = H_i(\omega)\varphi_i(x_P)\varphi_i(x)P(x_P)\delta(\omega-\omega_0) \ . \qquad (3.15)$$

In analogy, the contribution to the total acceleration, originating from the i'th mode, $\tilde{a}_i(x,\omega)$, is determined as

$$\tilde{a}_i(x,\omega) = -\omega^2\tilde{q}_i(\omega)\varphi_i(x) = -\omega^2 H_i(\omega)\varphi_i(x_P)\varphi_i(x)P(x_P)\delta(\omega-\omega_0) \ . \qquad (3.16)$$

The *accelerance*, $A(x,\omega)$, which is simply the transfer function between the force input and the derived acceleration of the structure, is now introduced. Combining the expressions (3.2), (3.14), and (3.16), we obtain

$$A(x,\omega) = -\omega^2\sum_{i=1}^{\infty} H_i(\omega)\varphi_i(x) \ . \qquad (3.17)$$

From the above, it is realized that even in the situation, where the structure is excited at a natural frequency $\omega_0 = \omega_k$, the accelerance response contain contributions from all off–resonant modes at that frequency[11], provided that the damping is larger than zero.

However, as it appears from (3.13), if the structure is lightly damped and the relevant natural frequency is well separated, in the sense that the off–resonant natural frequencies are far from the excited natural frequency, the contribution originating from the off–resonant modes will be moderate. Nevertheless, the peaks in the accelerance will not occur exactly at the natural frequencies, but at frequencies displaced slightly from those[12].

[11] In case of non–proportional damping, which is not described by the present equations, this effect is usually more pronounced, as the system of equations do not even decouple.

[12] Note that as the frequency response function is a complex quantity, the extremum of the accelerance can *not* be determined by considering the *amplitudes* of the resonant– and off–resonant contributions only, but the *phase angles* between those have to be taken into account as well.

Structures with the above characteristics behaves to a large extend as SDOF systems around the modal frequency and are known as simple structures[13].

The turbine blade structures are now presumed to be lightly damped[14] (but not so lightly damped that accurate measurements at resonance are difficult to obtain) with well–separated natural frequencies, which is often the situation.

In the vicinity of a resonance, the contributions to the response from the off–resonant modes are further completely neglected. Consequently, in a suitable frequency interval around a natural frequency ω_k, the deformation pattern thus appears as a true principal mode with the corresponding accelerance approximated by

$$A(x,\omega_e) = -\omega_e^2 H_k(\omega_e)\varphi_k(x) \; ; \qquad \left|\frac{\omega_k-\omega_e}{\omega_k}\right| \ll 1. \tag{3.18}$$

Introducing (3.13) into (3.18), the approximated accelerance is rewritten as

$$A(x,\omega_e) = \frac{\omega_e^2\varphi_k(x)[\omega_e^2-\omega_k^2+2j\omega_e\omega_k\xi_{sk}]}{m_k[(\omega_e^2-\omega_k^2)^2+4\omega_e^2\omega_k^2\xi_{sk}^2]} \; ; \qquad \left|\frac{\omega_k-\omega_e}{\omega_k}\right| \ll 1. \tag{3.19}$$

From the above, the modulus $|A(x,\omega_e)|$ and the phase $\psi(x,\omega_e)$ of the accelerance are easily determined as

$$|A(x,\omega_e)| = \frac{\omega_e^2|\varphi_k(x)|}{m_k\sqrt{(\omega_e^2-\omega_k^2)^2+4\omega_e^2\omega_k^2\xi_{sk}^2}} \; ; \qquad \left|\frac{\omega_k-\omega_e}{\omega_k}\right| \ll 1, \tag{3.20}$$

and

$$\psi(x,\omega_e) = \begin{cases} Arctan\left(\frac{2\omega_e\omega_k\xi_{sk}}{\omega_e^2-\omega_k^2}\right) & ; \; Re[A(x,\omega_e)] \geq 0 \\ Arctan\left(\frac{2\omega_e\omega_k\xi_{sk}}{\omega_e^2-\omega_k^2}\right)+\pi & ; \; Re[A(x,\omega_e)] < 0 \wedge Im[A(x,\omega_e)] > 0 \\ Arctan\left(\frac{2\omega_e\omega_k\xi_{sk}}{\omega_e^2-\omega_k^2}\right)-\pi & ; \; Re[A(x,\omega_e)] < 0 \wedge Im[A(x,\omega_e)] \leq 0 \end{cases} \tag{3.21}$$

where also in the last equation it is understood that $\left|\frac{\omega_k-\omega_e}{\omega_k}\right| \ll 1$. In the above, $Arctan(\cdot)$ denote the principal branch of the inverse tangent function, and the real– and imaginary part of the accelerance are given by

$$Re[A(x,\omega_e)] = \frac{\varphi_k(x)\omega_e^2(\omega_e^2-\omega_k^2)}{m_k[(\omega_e^2-\omega_k^2)^2+4\omega_e^2\omega_k^2\xi_{sk}^2]} \; ; \qquad \left|\frac{\omega_k-\omega_e}{\omega_k}\right| \ll 1, \tag{3.22}$$

and

$$Im[A(x,\omega_e)] = \frac{2\varphi_k(x)\omega_e^3\omega_k\xi_{sk}}{m_k[(\omega_e^2-\omega_k^2)^2+4\omega_e^2\omega_k^2\xi_{sk}^2]} \; ; \qquad \left|\frac{\omega_k-\omega_e}{\omega_k}\right| \ll 1. \tag{3.23}$$

It appears that $Re[A(x,\omega_e)]$ as well as $Im[A(x,\omega_e)]$ are proportional to the k'th normal mode $\varphi_k(x)$. If the particular mode shape has nodal points, then the

[13] A number of methods exist for analysing measured frequency response functions which, although different in their detail, all share the same basic assumption : in the vicinity of a resonance the total response is dominated by the contribution of the mode whose natural frequency is closest. The methods vary as to whether they assume that *all* the response is attributed to that single mode or whether the contributions from the off–resonant modes are taken into account by some simple approximation.

[14] Measurements have shown a logarithmic decrement for flap– and edgewise deflections of the order of magnitude 2% and 3%, respectively. This corresponds to damping ratios of the order of magnitude 0.003 and 0.005, respectively. Based on these measurements, the assumption seems to be well founded.

sign of the mode shape change when passing through such a nodal point. As a consequence, the sign of $Re[A(x,\omega_e)]$ as well as of $Im[A(x,\omega_e)]$ will change when passing through a nodal point, and from (3.21) this is seen to equivalate a shift in the phase of either π or $-\pi$.

At resonance, the approximated accelerance is especially simple due to the ballance between the inertia forces and the internal elastic forces. From expression (3.19) we derive

$$A(x,\omega_k) = \frac{j\varphi_k(x)}{2m_k\xi_{sk}} \ . \tag{3.24}$$

In this situation, the accelerance is seen to be purely imaginary with the phase $\frac{\pi}{2}$ for positive values of $\varphi_k(x)$ and $-\frac{\pi}{2}$ for negative values of $\varphi_k(x)$.

To proceed and determine the mode shape, we notice that the imaginary part of the accelerance $Im[A(x,\omega_e)]$, in the vicinity of the natural frequency ω_k, do not have any zero points, whereas the opposite just has been demonstrated for the real part. A non–zero proportionallity between $Im[A(x,\omega_e)]$ and the k'th normal mode has then been demonstrated. As a mode shape in its nature is determined apart from a constant, the imaginary part of the accelerance can be interpreted as the mode shape. Alternatively, this result can be normalized in some arbitrary chosen manner.

In practice, the determination of the accelerance is often based on digital sampling with a finite sampling rate. Therefore, it might not be possible to evaluate the accelerance exactly at the resonance frequency, but rather at a frequency ω_e slightly displaced from this. In this case, expression (3.23) demonstrate the importance of selecting the *same* frequency ω_e for all the x–values involved in an experimental determination of a mode shape – otherwise the proportionallity between the mode shape and the imaginary part of the accelerance will depend on x (as ω_e then depend on x), and a correction for this is not straight forward. Note from expression (3.21), that the assumption of lightly damped structural modes has the consequence that even slight displacements from a resonance frequency result in large changes in the phase angle corresponding to the resonance situation ($\frac{\pi}{2}$ or $-\frac{\pi}{2}$).

In the present investigation, a sinusoidal excitation has been chosen due to its favorable S/N ratio[15], and the posibility of control with both amplitude and frequency content. The method is rather time consuming, but in the present case it was manageable as only a few modes on each blade had to be investigated.

However, several other methods of exciting the structure exists, among which random excitation and impact excitation[16] are the most common. The above analysis procedure will apply also for these excitations types, as the accelerance is related to blade characteristics rather than to loading characteristics.

[15]This is due to the ability of input of a large amount of vibration energy at the relevant frequency.

[16]In an initial phase of the measuring campain, the impact loading was attempted with disappointing results.

3.1 Measurements on the LM17 m blade

The method sketched in the previous section is now applied to determine the flapwise and edgewise mode shapes of the LM17 m blade. Only the mode shapes corresponding to the lowest natural frequencies are considered in the present investigation.

Experimental setup

The LM17 m blade was mounted in a horizontal position, clamped to a rigid test stand at the root flange, and excited (close to the tip) by a sinusoidal point loading. The sinusoidal loading originated from a B&K vibration exciter, type 4809, connected to a B&K 2706 power amplifier and a Phillips PM5193 Programmable Synthesizer function generator, thus giving the possibility of controlling the frequency as well as the amplitude of the excitation.

The excitation could be applied in the flapwise as well as in the edgewise principal directions, and the magnitude of the applied force was measured by a force transducer mounted directly at the blade. The blade response, in terms of acceleration, was recorded by use of a piezoelectric B&K accelerometer, type 4370 . The signals from both force- and response transducers were, through charge preamplifiers, B&K type 2635, connected to a HP3582A Dual Channel Analyzer. The experimental setup is sketched on Fig. 23 below.

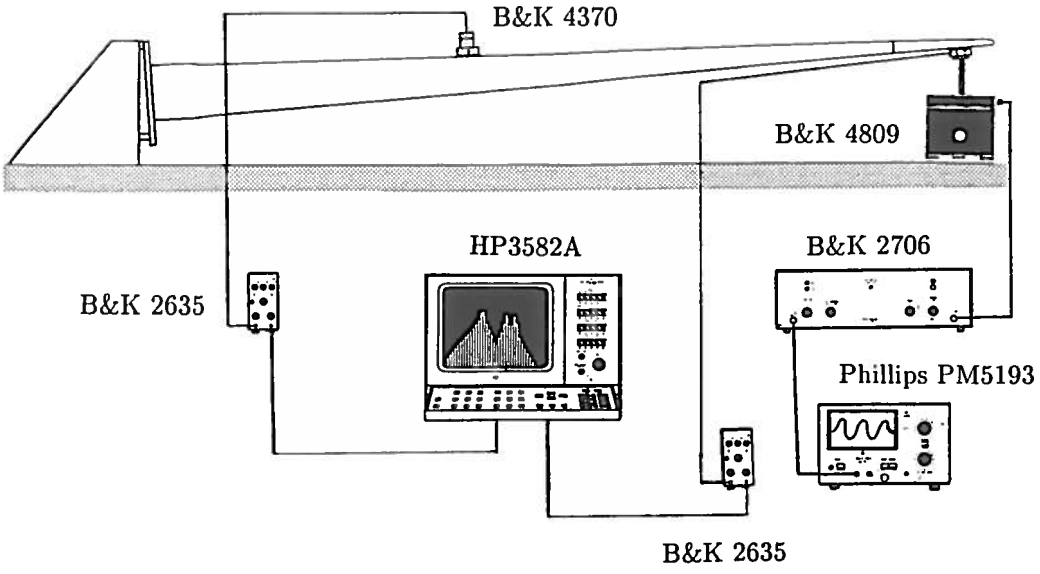

Figure 23. Modal analysis of a wind turbine blade.

Test procedure and results

Initially, a frequency sweep with the exciting force was performed in order to estimate the first flap- and edgewise natural frequencies. The accelerometer was

orientated to registrate the deflections in the excitation direction of current interest, but otherwise in an arbitrary position at the blade. Assuming well separated natural modes, the frequency, giving rise to the peak response[17], is considered a good approximation to the natural frequency. However, as pointed out in the previous section, the extremum of the response does not correspond exactly to the particular natural frequency. By this method, first flapwise and edgewise natural frequencies were estimated to 1.975 Hz and 3.575 Hz, respectively. This is slightly below the values[18] obtained from free vibration tests.

The second step is to excite the structure, in the appropriate direction, by a force with a (constant) frequency, equal to the natural frequency of the mode to be investigated, and subsequently to record the response at different points (spaced with a suitable resolution) along the blade. In the present test, the response has been measured in 62 locations by moving the accelerometer around. Most of the measuring stations were equally spaced with 0.25 m between them.

By use of the HP3582A analyzer, the modulus as well as the phase of the peak accelerance have been extracted for each of the measuring stations. In order to improve the statistical significance of the measured data, the determination of the accelerance has been based on spectral averaging. The number of successive frequency spectra, to be combined in the averaging procedure, ranged between 3 and 8, depending on the signal, as more points were required for small signals.

The results related to the first flapwise and edgewise natural modes are listed in Appendix E and in Appendix F, respectively. As shown in section 3, the imaginary part of the complex accelerance determines the modal value at a particular measuring station, and this quantity is also listed in the appendices.

The measured first flapwise and edgewise modes are shown in Fig.24 and Fig.25.

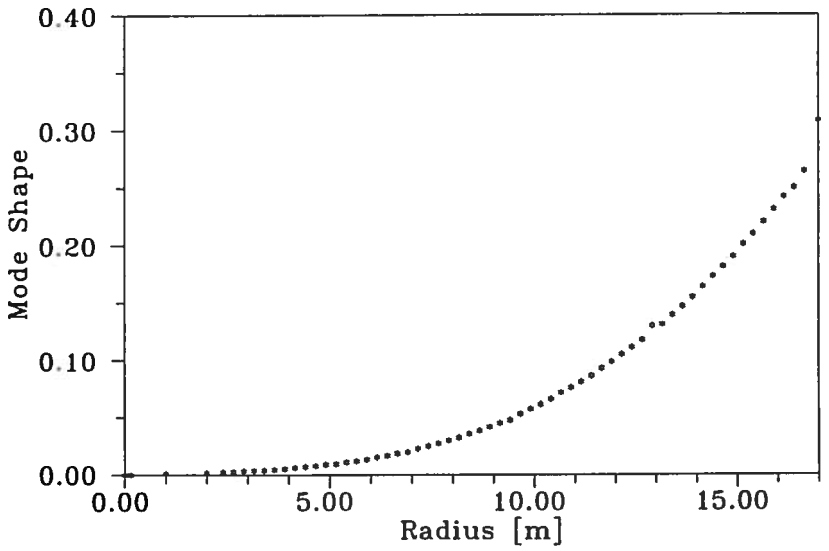

Figure 24. Measured first flapwise mode of the LM17 m blade.

[17] Presumed that the amplitude of the exciting force is kept constant.

[18] In free vibration tests, the first flapwise and edgewise natural frequencies were measured to 2.08 Hz and 3.68 Hz, respectively.

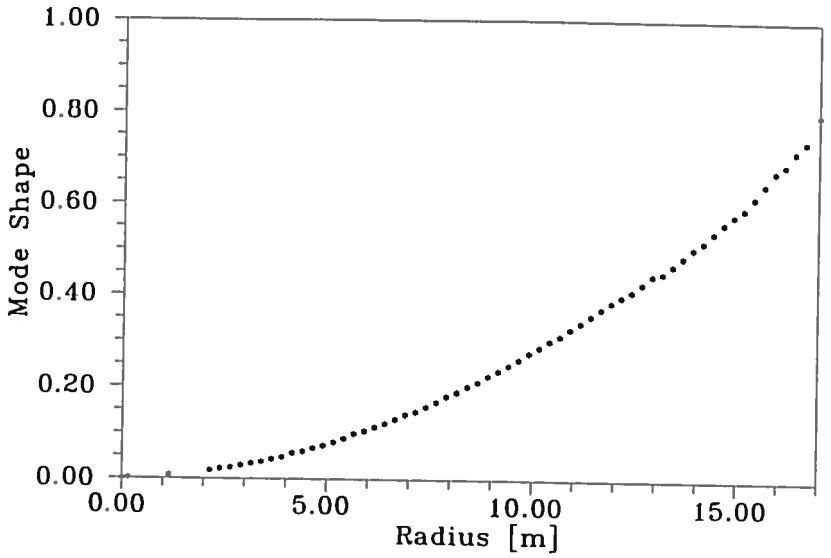

Figure 25. Measured first edgewise mode of the LM17 m blade.

As seen, the curves display a "nice" smooth appearance with very little scatter.

3.2 Measurements on the LM19 m blade

The subject for the present subsection is the determination of mode shapes related to the LM19 m blade. The first and second flapwise modes and the first edgewise mode have been measured. The experimental setup and the test procedure were the same as the ones applied for the determination of the mode shapes related to the LM17 m blade.

Results

Assuming well separated natural modes, the first and second flapwise natural frequencies have been estimated to 1.80 Hz and 5.68 Hz, respectively. The first edgewise natural frequency was estimated to 2.80 Hz.

The acceleration response to the relevant sinusoidal excitation has been measured at 66, 67, and 68 stations for the first flapwise–, the first edgewise–, and the second flapwise mode, respectively. As with the LM17 m blade, most of the measuring stations were equally spaced with 0.25 m between them.

The modulus and the phase of the peak accelerance have been extracted for each of the measuring stations, and the results for the flapwise– and the edgewise modes are given in Appendix G and in Appendix H, respectively. As with the LM17 m blade registrations, the statistical significance of the accelerance has been improved by use of spectral averaging. In the present situation between 3 and 5 successive frequency spectra have been combined in the averaging procedure. The mode shape values, in terms of the imaginary part of the accelerance, are also presented in the appendices.

The measured first flapwise–, second flapwise–, and first edgewise mode are shown in Fig.26, Fig.27, and Fig.28, respectively.

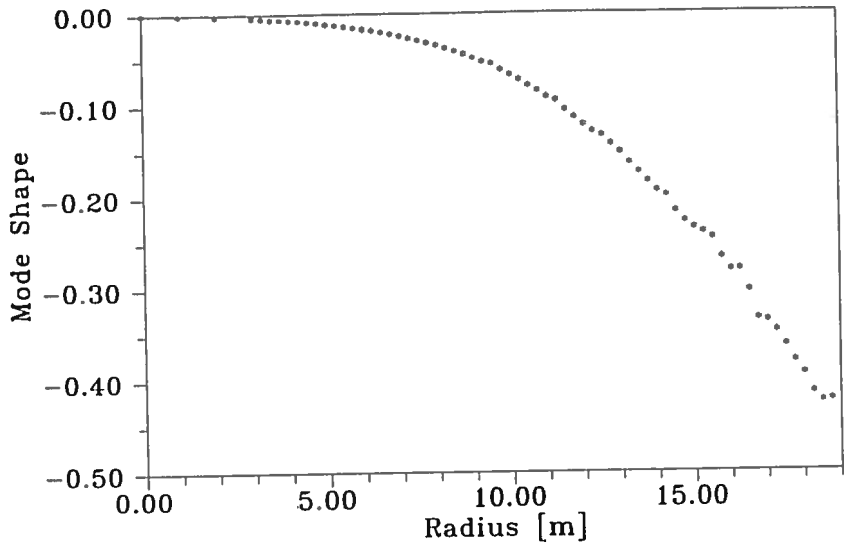

Figure 26. Measured first flapwise mode of the LM19 m blade.

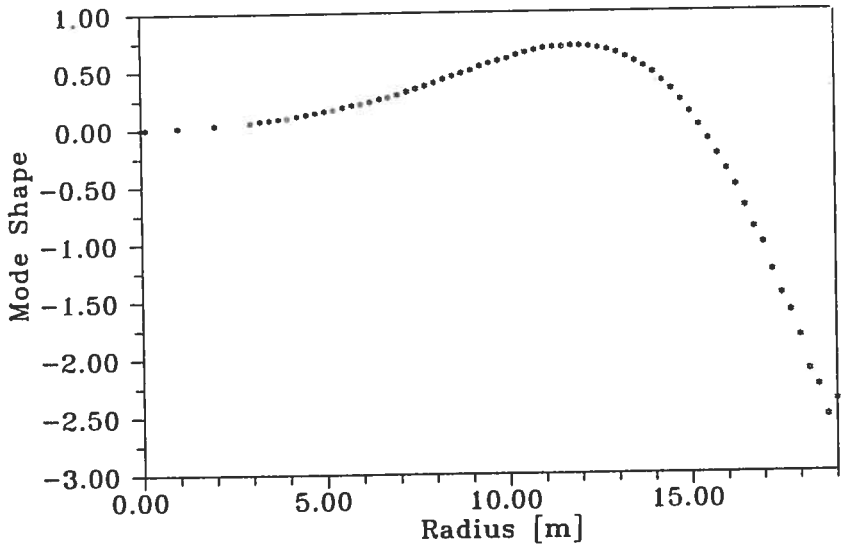

Figure 27. Measured second flapwise mode of the LM19 m blade.

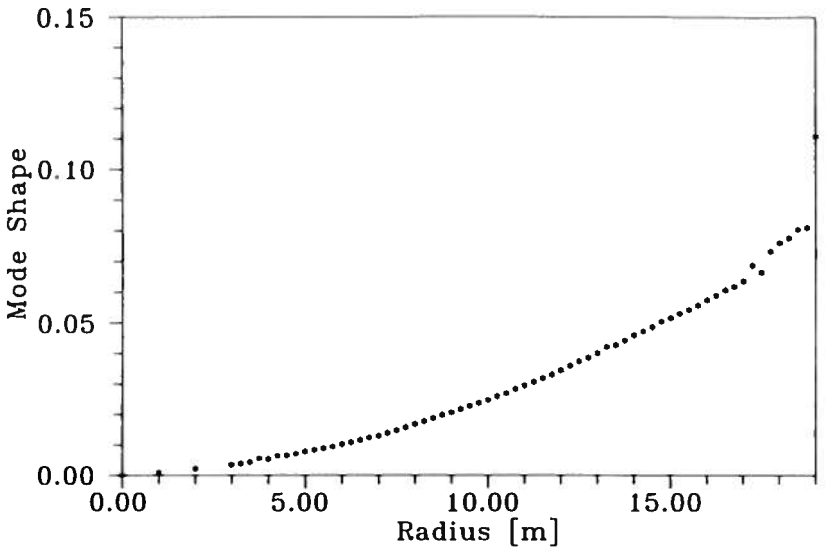

Figure 28. Measured first edgewise mode of the LM19 m blade.

As with the modal results related to the LM17 m blade, the estimated mode shapes related to the LM19 m blade are "nice" smooth curves with very little scatter. Moreover, the data related to the second flapwise mode reveal, with good approximation, the expected phase shift of 180 degrees in the accelerance when passing through the node of this mode shape. Note furthermore, from the values presented in the appendices, that the phase angles, as expected, differ considerable from the value related to the pure resonance situation.

3.3 Evaluation of results

It has been demonstrated that the described method produces mode shape results with a very smooth apperance. Other qualitative appealing features are that the determined mode shapes seem to have a horizontal tangent at the clamped end, and that the expected phase shift of 180 degrees in the accelerance, when passing through a modal node, is revealed with good accuracy.

The uncertainty, introduced by misalignment of the accelerometers with the direction of the vibration, is considered to be less than 1 % corresponding to a misalignment of the order of magnitude 8 degrees, and is thus of no importance.

In order to obtain a more quantitative measure of the quality of the method, a redundance in the data material for the LM17 m blade has been utilized to check the mutual overall consistence between the obtained experimental results.

It is well known, see e.g. Larsen et. al. [4], that a natural frequency can be expressed in terms of generalized mass- and stiffness quantities as

$$\omega_k = \sqrt{\frac{k_k}{m_k}}\,, \tag{3.25}$$

with the generalized mass defined by (3.7), and the generalized stiffness expressed

by

$$k_k = \int_0^L E(x)I(x)\left(\frac{\partial^2 \varphi_k(x)}{\partial x^2}\right)^2 dx \ , \tag{3.26}$$

where $\varphi_k(x)$ denotes the mode shape corresponding to the k'th natural frequency.

The estimated mass distribution, flapwise stiffness distribution, and first flapwise mode shape for the LM 17 m blade can be substituted into the above relations, and the resulting frequency estimate can then be compared with the measured first flapwise natural frequency. In [1], the estimated mass distribution has been demonstrated to be in very good agreement with the exact mass distribution, and in section 2.5 good agreement between calculated and experimentally determined flexural rigidities of the LM17 m blade has been found. It is consequently resonable to consider the above comparison as a measure of the quality of the measured mode shape.

The determination of the second derivative of a measured mode shape is critical. Therefore, the measured mode shape has been smoothed according to expression (2.4) with $N = 3$. The first flapwise natural frequency has been measured to $\omega_m = 2.08$ Hz, and estimated from (3.25) to $\omega_{est} = 2.22$ Hz, which equivalate a relative deviation of the order of magnitude 6%. The agreement is considered satisfactory, and consequently the quality of the measured first flapwise mode shape, related to the LM17 m blade, has been demonstrated.

The quantitative check has only been applied to results related to the LM17 m blade as a measured mass distribution is available only for this blade. Moreover, only the flapwise mode has been considered as the flexural rigidity in the root part of the blade is poorly determined for the edgewise deflection. However, as the experimental method is identical and as no individual difficulties are envisaged in relation to the determination of the remaining mode shapes, the quantitative check is considered to some extend also to validate these.

4 Conclusion

Two non-destructive experimental methods, related to the structural properties of wind turbine blades, have been formulated and applied to two different blades.

The first method deals with the determination of the flexural rigidities of wind turbine blades, and is based on static deflection measurements. The procedure has been applied to determine the distribution of flapwise- and edgewise flexural rigidities of the LM17 m and the LM19 m blade. The results have been compared to results obtained from cross section calculations, and the overall agreement between measured and calculated flapwise flexural rigidities is good, indicating that the measuring procedure is not significantly distorted by effects as local buckling of the surface, creep in the material, or coupling between bending and torsion in the pretwisted blade. However, the resolution of the deformation in the blade part close to the root was not sufficient to enable a determination of the flexural rigidity here, but this could be compensated for by increasing the loading. The agreement between measured- and calculated edgewise rigidities for the LM17 m blade is satisfactory. However, the insufficient resolution in the root part is even more pronounced here than in the flap-situation. Concerning the edgewise rigidities of the LM19 m blade some deviation is observed, and the poor resolution of the curvature in the root part is difficult to circumvent in this situation due to the seemingly hinge like deformation mechanism. To cope with that, a strain-gauge based method might be considered in the future.

The second method deals with the determination of blade mode shapes corresponding to the natural frequencies. The method is founded on an experimental determination of the transfer function, relating a dynamic loading with the corresponding acceleration response, in a suitable number of points along the structure. The method has been used to determine the first flapwise and edgewise natural modes of the LM17 m blade, and the natural modes of the LM19 m blade related to the first flapwise-, second flapwise-, and first edgewise natural frequency. It has been demonstrated that the described method produces mode shape results with a very smooth apperance. Other qualitative appealing features are that the determined mode shapes seem to have a horizontal tangent at the clamped end, and that the expected phase shift of 180 degrees in the accelerance, when passing through a modal node, is revealed with good accuracy. Finally, a qualitative test of the LM17 m first flapwise mode has been performed by comparing the ratio between the generalized mass and stiffness, based on the experimentally determined mode shape, to the square of the relevant natural frequency. A relative deviation of the order of magnitude 6% was obtained which is considered satisfactory. The quantitative check has only been applied to results related to the first flapwise mode related to the LM17 blade. However, as the experimental method is identical and as no individual difficulties are envisaged in relation to the determination of the remaining mode shapes, the quantitative check is considered to some extend also to validate these. The method has revealed a marginal influence from non-resonance modes, as the peak accelerance differ slightly from the values of the natural frequencies obtained from free vibration tests. The influence from non-resonance modes might be more pronounced for other modes and/or blades. In this situation, it is possible to refine the method either by isolating the relevant mode shape by application of multi-exciter methods or by combining the present single-exciter method with a more advanced analytical treatment[19].

[19] Based on the behaviour of the accelerance as a function of frequency, it is possible to construct a analytical "filter" to separate the relevant mode shape from a combined signal containing (significant) contributions from off-resonance modes.

Acknowledgements

Erik Grove Nielsen and Hans Lund-Thomsen are acknowledged for their helpfulness during the measuring campains, which was conducted at The Test Stations blade test center in Sparkær, Viborg. Thanks are also due to Stener Hansen at The Test Station for his effort concerning the production of a holder to the vibration exciter with short respite.

References

[1] Larsen, G. C. (1995). Linear Chi-Square Fit of a Blade Mass Distribution. Risø-R-772. Risø National Laboratory, Denmark.

[2] Ewins, D. J. (1986). Modal testing: Theory and Practice. Research Studies Press Ltd. and Brüel & Kjær.

[3] Zaveri, M. (1984). Modal Analysis of Large Structures – Multible Exciter Systems. Brüel & Kjær, Denmark.

[4] Larsen, G. C. et. al. (1989). Design Basis for Horizontal Axis Wind Turbines – Theoretical Background. Risø-M-2836. Risø National Laboratory, Denmark.

A Measured flapwise deflection data for the LM17 m blade

The present appendix concerns the measured flapwise deflections related to the LM17 m blade. In order to obtain a satisfactory resolution of the deflections in all points along the blade, and at the same time to respect the limited load carrying capacity in the tip region of the blade, a series of relatively large vertical point forces and a series of relatively small vertical point forces have applied to the clamped blade at the positions defined by $x_P = 11.47\ m$ and $x_P = 14.90\ m$, respectively.

In Table A.1, the measured deflection data, related the point of attack $x_P = 11.47\ m$, are listed, and Table A.2 contains the deflection data corresponding to the point of attack defined by $x_P = 14.90\ m$. In both tables, the first column defines the measuring stations, whereas the following columns contain the measured positions of the blade surface (relative to a fixed reference) together with specifications of the values of the applied forces.

The specification $P = 0$ defines the unloaded situation, and the deflection, caused by a given loading, is then obtained by subtracting the blade surface position values, corresponding to the unloaded situation, from the blade surface position values corresponding to the relevant loading.

Table A.1. Measured blade surface position data originating from the application of vertical point forces at the position defined by $x_P = 11.47\ m$.

x [m]	surface position ($P = 0$) [mm]	surface position ($P = 13748\ N$) [mm]	surface position ($P = 20622\ N$) [mm]	surface position ($P = 26219\ N$) [mm]
2.40	117.0	115.0	114.0	113.0
2.65	135.0	132.0	131.0	131.0
2.90	150.0	148.0	146.0	145.0
3.15	168.0	165.0	163.5	162.5
3.40	184.0	180.0	179.0	177.5
3.65	200.0	196.0	193.0	192.0
3.90	214.0	209.0	206.0	205.0
4.15	227.0	222.0	218.0	216.0
4.40	240.0	232.0	229.0	226.0
4.65	251.0	243.0	239.0	236.0
4.90	262.0	252.0	247.0	244.0
5.15	274.0	263.0	257.5	253.5
5.40	283.0	270.0	264.0	259.5
5.65	293.0	278.0	271.0	266.0
5.90	302.0	286.0	277.5	271.0
6.15	311.0	292.0	283.0	276.0
6.40	318.0	297.0	287.0	278.0
6.65	326.0	302.0	291.0	282.0
6.90	331.0	305.0	292.0	282.0
7.15	336.0	306.0	292.5	281.0
7.40	341.0	310.0	293.0	281.0
7.65	347.0	311.0	293.0	280.0
7.90	352.0	312.0	292.0	278.0
8.15	356.0	312.0	291.0	274.0
8.40	359.0	311.0	288.0	269.0
8.65	362.0	310.0	284.0	264.0
8.90	364.0	306.0	280.0	258.0
9.15	366.0	305.0	274.0	250.0
9.40	367.0	300.0	268.0	241.0
9.65	368.0	296.0	260.0	232.0
9.90	369.0	291.0	252.0	221.5
10.15	370.0	286.0	243.0	211.0
10.40	370.0	279.0	235.0	200.0
10.65	370.0	272.0	225.0	185.0
10.90	370.0	266.0	215.0	175.0

Table A.2. Measured blade surface position data originating from the application of vertical point forces at the position defined by $x_P = 14.90\ m$.

x [m]	surface position ($P = 0$) [mm]	surface position ($P = 2386\ N$) [mm]	surface position ($P = 4959\ N$) [mm]	surface position ($P = 6540\ N$) [mm]
7.15	353.0	346.0	338.0	334.0
7.40	357.5	350.0	341.0	336.0
7.65	362.0	352.0	344.0	339.0
7.90	365.0	355.0	344.5	339.0
8.15	367.0	357.0	345.0	337.5
8.40	370.0	357.5	345.0	337.0
8.65	371.0	358.0	343.0	335.0
8.90	372.0	357.5	342.0	332.0
9.15	373.0	356.5	340.0	329.0
9.40	373.0	355.0	336.0	325.0
9.65	373.0	353.0	332.0	320.0
9.90	372.0	351.0	327.5	315.0
10.15	372.0	348.0	323.0	308.5
10.40	371.0	345.0	318.0	301.0
10.65	369.0	341.0	312.0	294.0
10.90	368.0	337.5	306.0	286.0
11.15	366.0	333.5	299.0	278.5
11.40	365.0	330.0	293.0	271.0
11.65	365.0	327.0	287.0	262.5
11.90	363.0	323.0	279.5	254.0
12.15	362.0	318.0	271.5	243.5
12.40	361.0	313.0	263.0	232.5
12.65	358.0	307.0	253.0	221.0
12.90	351.0	296.5	239.0	204.5
13.15	354.0	296.0	234.0	197.0
13.40	351.0	288.5	223.0	183.0
13.65	347.5	281.0	211.0	168.0
13.90	344.0	273.0	199.0	153.5
14.15	341.0	265.0	186.0	137.0
14.40	338.0	256.5	173.0	121.0

B Measured edgewise deflection data for the LM17 m blade

The present appendix concerns the measured edgewise deflections related to the LM17 m blade. In order to obtain a satisfactory resolution of the deflections in all points along the blade, and at the same time to respect the limited load carrying capacity in the tip region of the blade, a series of relatively large vertical point forces and a series of relatively small vertical point forces have applied to the clamped blade at positions defined by $x_P = 10.00\ m$ and $x_P = 16.65\ m$, respectively.

In Table B.1, the measured deflection data, related the point of attack $x_P = 10.00\ m$, are listed, and Table B.2 contains the deflection data corresponding to the point of attack defined by $x_P = 16.65\ m$. In both tables, the first column defines the measuring stations, whereas the following columns contain the measured positions of the blade surface (relative to a fixed reference) together with specifications of the values of the applied forces.

The specification $P = 0$ defines the unloaded situation, and the deflection, caused by a given loading, is then obtained by subtracting the blade surface position values, corresponding to the unloaded situation, from the blade surface position values corresponding to the relevant loading.

Table B.1. Measured blade surface position data originating from the application of vertical point forces at the position defined by $x_P = 10.00\ m$.

x [m]	surface position ($P = 0$) [mm]	surface position ($P = 13748\ N$) [mm]	surface position ($P = 15417\ N$) [mm]	surface position ($P = 20818\ N$) [mm]
2.40	559.5	556.5	556.5	556.5
2.65	555.5	553.0	551.5	551.5
2.90	559.5	555.0	557.0	553.5
3.15	563.0	556.5	554.5	555.0
3.40	567.0	559.0	557.5	557.0
3.65	570.0	561.5	561.0	558.5
3.90	574.0	564.0	564.0	561.0
4.15	579.0	567.5	567.0	564.0
4.40	582.0	571.0	570.0	567.5
4.65	587.5	575.0	574.5	570.0
4.90	592.0	579.0	576.5	573.0
5.15	597.0	585.0	580.5	577.0
5.40	230.5	219.0	218.0	214.0
5.65	235.5	222.5	222.0	212.5
5.90	240.0	227.5	226.0	220.5
6.15	246.0	231.5	230.5	224.5
6.40	251.5	236.0	235.0	228.5
6.65	257.5	241.0	239.5	233.0
6.90	264.0	247.0	245.0	238.0
7.15	270.0	250.5	249.0	241.5
7.40	275.0	255.5	253.5	245.5
7.65	281.0	259.0	258.0	250.0
7.90	287.0	264.5	262.0	254.0
8.15	293.5	268.5	266.5	258.0
8.40	299.0	273.5	271.0	261.5
8.65	304.5	277.5	275.0	265.5
8.90	310.5	281.0	280.0	269.0
9.15	316.5	287.0	285.0	273.0
9.40	324.5	292.0	289.0	275.5
9.65	339.0	298.0	296.5	284.0

Table B.2. Measured blade surface position data originating from the application of vertical point forces at the position defined by $x_P = 16.65\ m$.

x [m]	surface position ($P = 0$) [mm]	surface position ($P = 2386\ N$) [mm]	surface position ($P = 3938\ N$) [mm]	surface position ($P = 5234\ N$) [mm]
5.40	0.0	-3.5	-6.0	-6.5
5.65	0.0	-4.5	-6.5	-8.5
5.90	0.0	-4.0	-7.0	-8.0
6.15	0.0	-5.0	-8.0	-9.0
6.40	0.0	-5.0	-8.0	-10.5
6.65	0.0	-5.5	-8.5	-11.0
6.90	0.0	-5.5	-8.5	-11.5
7.15	0.0	-6.5	-10.0	-12.5
7.40	0.0	-6.5	-11.0	-14.0
7.65	0.0	-7.0	-11.0	-14.5
7.90	0.0	-8.0	-12.5	-16.0
8.15	0.0	-8.5	-14.0	-17.5
8.40	0.0	-9.5	-15.0	-18.0
8.65	0.0	-10.0	-16.0	-19.5
8.90	0.0	-12.0	-18.5	-24.5
9.15	0.0	-11.0	-17.5	-22.5
9.40	0.0	-12.0	-19.5	-25.0
9.65	0.0	-11.0	-18.0	-24.0
9.90	0.0	-13.0	-21.0	-26.5
10.15	0.0	-14.0	-23.0	-28.0
10.40	0.0	-14.0	-22.5	-29.0
10.65	0.0	-14.0	-23.5	-30.5
10.90	0.0	-15.5	-25.5	-32.5
11.15	0.0	-16.0	-26.5	-34.5
11.40	0.0	-17.0	-28.0	-34.5
11.65	0.0	-17.0	-28.5	-35.5
11.90	0.0	-18.0	-29.5	-38.5
12.15	0.0	-18.5	-30.5	-40.5
12.40	0.0	-19.5	-32.5	-43.0
12.65	0.0	-20.0	-34.0	-44.0
12.90	0.0	-21.0	-36.0	-47.5
13.15	0.0	-24.0	-39.0	-50.0
13.40	0.0	-24.0	-39.5	-51.5
13.65	0.0	-25.0	-41.5	-54.5
13.90	0.0	-25.0	-42.5	-56.0
14.15	0.0	-28.0	-45.0	-59.5
14.40	0.0	-29.0	-48.0	-62.5
14.65	0.0	-29.5	-49.0	-64.5
14.90	0.0	-31.0	-52.0	-69.0
15.15	0.0	-34.5	-56.5	-74.5
15.40	0.0	-39.0	-63.0	-83.0
15.65	0.0	-42.5	-68.5	-89.5
15.90	0.0	-46.0	-74.0	-97.5
16.15	0.0	-50.0	-81.0	-107.0

C Measured flapwise deflection data for the LM19 m blade

The present appendix contains the measured flapwise deflections related to the LM19 m blade. In order to obtain a satisfactory resolution of the deflections in all points along the blade, and at the same time to respect the limited load carrying capacity in the tip region of the blade, a series of relatively large vertical point forces and a series of relatively small vertical point forces have applied to the clamped blade at positions defined by $x_P = 13.07\ m$ and $x_P = 18.50\ m$, respectively.

In Table C.1, the measured deflection data, related the point of attack $x_P = 13.07\ m$, are listed, and Table C.2 contains the deflection data corresponding to the point of attack defined by $x_P = 18.50\ m$. In both tables, the first column defines the measuring stations, whereas the following columns contain the measured positions of the blade surface (relative to a fixed reference) together with specifications of the values of the applied forces.

The specification $P = 0$ defines the unloaded situation, and the deflection, caused by a given loading, is then obtained by subtracting the blade surface position values, corresponding to the unloaded situation, from the blade surface position values corresponding to the relevant loading.

Table C.1. Measured blade surface position data originating from the application of vertical point forces at the position defined by $x_P = 13.07\ m$.

x [m]	surface position ($P = 0$) [mm]	surface position ($P = 9820\ N$) [mm]	surface position ($P = 16989\ N$) [mm]	surface position ($P = 23470\ N$) [mm]
3.00	74.0	71.0	69.0	66.0
3.25	89.0	84.0	82.0	80.0
3.50	102.5	98.5	95.0	92.0
3.75	117.0	111.5	108.0	105.0
4.00	130.0	124.0	121.0	117.0
4.25	144.0	136.5	132.5	128.5
4.50	158.0	149.5	145.5	140.5
4.75	172.0	163.5	157.5	153.5
5.00	186.0	176.0	171.0	165.0
5.25	201.0	190.0	182.5	177.0
5.50	212.0	201.5	194.0	187.0
5.75	227.0	213.5	205.0	197.0
6.00	239.0	224.5	215.0	207.0
6.25	250.5	234.0	224.0	215.0
6.50	261.0	243.5	232.0	222.0
6.75	271.5	252.0	240.0	229.0
7.00	281.0	260.5	246.0	233.5
7.25	291.0	268.5	253.0	239.0
7.50	300.0	275.0	258.5	243.5
7.75	308.0	281.0	263.0	246.5
8.00	316.0	286.0	266.5	248.0
8.25	322.0	291.0	269.5	250.0
8.50	328.0	293.5	270.5	249.0
8.75	332.0	294.5	269.0	245.0
9.00	336.0	295.5	267.5	242.5
9.25	341.0	296.5	267.0	239.0
9.50	346.0	297.5	265.0	235.0
9.75	349.5	297.5	263.0	230.5
10.00	353.0	297.0	260.0	224.0
10.25	355.0	294.5	254.0	212.0
10.50	357.0	291.5	247.5	207.5
10.75	358.0	288.0	240.0	197.5
11.00	358.0	282.0	231.5	185.0
11.25	359.0	278.0	223.5	174.0
11.50	360.0	273.0	215.0	162.5
11.75	360.0	268.0	205.5	149.0
12.00	360.0	262.0	195.5	134.5
12.25	360.0	255.0	184.0	120.5
12.50	359.0	248.0	173.0	105.0

Table C.2. Measured blade surface position data originating from the application of vertical point forces at the position defined by $x_P = 18.50\ m$.

x $[m]$	surface position ($P = 0$) $[mm]$	surface position ($P = 1954\ N$) $[mm]$	surface position ($P = 3064\ N$) $[mm]$	surface position ($P = 4939\ N$) $[mm]$
5.00	186.0	185.5	181.5	180.0
5.25	201.0	198.0	196.5	193.0
5.50	212.0	211.0	208.0	205.0
5.75	227.0	223.0	220.0	217.5
6.00	239.0	236.0	232.0	230.0
6.25	250.5	247.0	243.0	240.0
6.50	261.0	257.0	253.0	249.0
6.75	271.5	266.5	263.0	258.0
7.00	281.0	276.0	272.0	266.5
7.25	291.0	284.5	281.0	275.5
7.50	300.0	298.5	289.0	282.5
7.75	308.0	300.5	295.5	289.0
8.00	316.0	307.0	302.0	294.5
8.25	322.0	314.0	309.0	300.0
8.50	328.0	318.5	313.0	303.5
8.75	332.0	321.0	315.0	304.5
9.00	336.0	324.5	317.0	306.0
9.25	341.0	328.0	319.5	308.0
9.50	346.0	332.0	323.0	309.5
9.75	349.5	334.5	325.0	310.0
10.00	353.0	338.0	326.0	310.0
10.25	355.0	337.5	325.0	308.5
10.50	357.0	337.0	324.0	305.5
10.75	358.0	336.5	322.0	301.5
11.00	358.0	334.5	319.5	296.5
11.25	359.0	332.5	315.5	292.0
11.50	360.0	331.5	314.0	286.0
11.75	360.0	329.5	311.0	280.5
12.00	360.0	327.0	307.0	274.0
12.25	360.0	323.5	302.0	266.5
12.50	359.0	320.0	296.5	259.0
12.75	358.0	315.5	290.0	249.0
13.00	955.0	909.0	882.5	838.0
13.25	954.0	904.0	873.5	827.0
13.50	952.0	898.0	866.5	816.0
13.75	950.0	892.5	857.0	803.0
14.00	947.0	885.0	847.5	789.0
14.25	943.5	877.5	837.0	773.5
14.50	940.0	870.0	827.5	758.5

Table C.2. (cont.) Measured blade surface position data originating from the application of vertical point forces at the position defined by $x_P = 18.50\ m$.

x [m]	surface position ($P = 0$) [mm]	surface position ($P = 1954\ N$) [mm]	surface position ($P = 3064\ N$) [mm]	surface position ($P = 4939\ N$) [mm]
14.75	954.5	878.0	833.0	758.5
15.00	933.0	850.0	802.0	722.0
15.25	929.0	840.5	786.5	703.0
15.50	925.0	829.5	773.5	682.0
15.75	921.0	819.0	759.0	661.0
16.00	917.0	809.0	747.0	641.0
16.25	913.5	798.0	731.0	620.0
16.50	909.0	786.0	713.0	595.5
16.75	907.5	775.5	698.0	571.0
17.00	903.5	762.0	679.0	545.0
17.25	902.0	751.0	666.0	521.0
17.50	904.0	743.0	649.0	495.0
17.75	904.5	732.0	632.0	466.0
18.00	903.5	719.0	611.0	434.5
18.25	903.0	705.0	590.0	400.0

D Measured edgewise deflection data for the LM19 m blade

The present appendix concerns the measured edgewise deflections related to the LM19 m blade. In order to obtain a satisfactory resolution of the deflections in all points along the blade, and at the same time to respect the limited load carrying capacity in the tip region of the blade, a series of relatively large vertical point forces and a series of relatively small vertical point forces have applied to the clamped blade at positions defined by $x_P = 13.07\ m$ and $x_P = 18.50\ m$, respectively.

In Table D.1, the measured deflection data, related the point of attack $x_P = 13.97\ m$, are listed, and Table D.2 contains the deflection data corresponding to the point of attack defined by $x_P = 18.50\ m$. In both tables, the first column defines the measuring stations, whereas the following columns contain the measured positions of the blade surface (relative to a fixed reference) together with specifications of the values of the applied forces.

The specification $P = 0$ defines the unloaded situation, and the deflection, caused by a given loading, is then obtained by subtracting the blade surface position values, corresponding to the unloaded situation, from the blade surface position values corresponding to the relevant loading.

Table D.1. Measured blade surface position data originating from the application of vertical point forces at the position defined by $x_P = 13.07\ m$.

x [m]	surface position ($P = 0$) [mm]	surface position ($P = 7070\ N$) [mm]	surface position ($P = 14926\ N$) [mm]	surface position ($P = 21506\ N$) [mm]	surface position ($P = 30737\ N$) [mm]
3.00	285.0	284.0	282.0	280.0	278.0
3.25	287.0	286.0	285.0	282.0	279.5
3.50	290.0	288.0	286.0	284.0	280.0
3.75	294.0	292.0	288.0	286.0	282.5
4.00	298.0	296.0	293.0	289.0	285.0
4.25	304.0	301.0	297.0	294.0	290.0
4.50	309.0	306.0	302.0	298.0	293.0
4.75	315.0	313.0	307.0	302.5	297.0
5.00	321.0	317.0	311.0	307.0	300.0
5.25	327.0	321.0	315.0	311.0	303.0
5.50	332.0	326.0	319.0	315.0	308.0
5.75	339.0	331.0	324.0	318.0	310.0
6.00	342.0	335.0	328.0	321.5	312.0
6.25	347.0	340.0	332.0	324.5	315.0
6.50	352.0	344.0	336.0	328.0	319.0
6.75	356.0	349.0	340.0	331.0	320.5
7.00	362.0	354.0	344.0	335.0	323.0
7.25	368.0	359.0	348.0	338.0	325.5
7.50	374.0	363.0	351.0	341.0	327.0
7.75	379.0	368.0	355.0	345.0	329.0
8.00	385.0	372.0	359.0	348.0	331.0
8.25	390.0	377.0	363.0	351.0	333.0
8.50	396.0	382.0	367.0	354.0	335.0
8.75	402.0	387.0	371.0	357.0	337.0
9.00	408.0	392.0	374.0	360.0	339.0
9.25	414.0	397.0	378.0	363.0	341.0
9.50	419.0	402.0	382.0	366.0	342.0
9.75	425.0	406.0	385.0	369.0	343.0
10.00	431.0	411.0	389.0	373.0	344.0
10.25	436.0	415.0	392.0	374.0	345.0
10.50	441.0	419.0	395.0	375.0	346.0
10.75	446.0	423.0	398.0	377.0	347.0
11.00	452.0	428.0	402.0	379.0	348.0
11.25	459.0	434.0	406.0	382.0	348.5
11.50	465.0	439.0	409.0	384.0	349.0
11.75	471.0	444.0	412.0	386.0	350.0
12.00	476.0	449.0	416.0	389.0	351.0
12.25	482.0	453.0	420.0	392.0	352.0
12.50	488.0	457.0	422.0	394.0	353.0

Table D.2. Measured blade surface position data originating from the application of vertical point forces at the position defined by $x_P = 18.50\ m$.

x $[m]$	surface position $(P = 0)$ $[mm]$	surface position $(P = 2966\ N)$ $[mm]$	surface position $(P = 3948\ N)$ $[mm]$	surface position $(P = 5440\ N)$ $[mm]$
5.00	321	318	319	317
5.25	327	323	322	321
5.50	332	328	327	325
5.75	339	334	333	330
6.00	342	338	337	333
6.25	347	342	341	338
6.50	352	347	345	343
6.75	356	351	350	347
7.00	362	357	354	351
7.25	368	362	360	357
7.50	374	367	364	361
7.75	379	372	369	365
8.00	385	376	374	369
8.25	390	381	379	374
8.50	396	387	384	379
8.75	402	392	389	384
9.00	408	396	393	388
9.25	414	402	399	393
9.50	419	407	403	396
9.75	425	413	407	401
10.00	431	418	412	406
10.25	436	422	417	410
10.50	441	427	421	414
10.75	446	430	425	417
11.00	452	436	430	423
11.25	459	442	435	430
11.50	465	447	439	432
11.75	471	452	444	438
12.00	476	457	449	439
12.25	482	462	453	444
12.50	488	465	458	447
12.75	494	472	462	450
13.00	497	472	464	457
13.25	506	490	475	460
13.50	514	491	476	467
13.75	521	492	482	468
14.00	527	497	486	471
14.25	534	504	490	475
14.50	539	508	495	479

Table D.2. Measured blade surface position data originating from the application of vertical point forces at the position defined by $x_P = 18.50\ m$.

x $[m]$	surface position $(P = 0)$ $[mm]$	surface position $(P = 2966\ N)$ $[mm]$	surface position $(P = 3948\ N)$ $[mm]$	surface position $(P = 5440\ N)$ $[mm]$
14.75	545	513	500	482
15.00	552	517	505	485
15.25	559	522	509	490
15.50	566	526	514	494
15.75	574	533	519	499
16.00	581	539	525	504
16.25	590	546	533	510
16.50	599	551	536	511
16.75	611	558	542	516
17.00	621	565	547	521
17.25	635	574	554	526
17.50	650	584	564	534
17.75	672	603	580	546
18.00	700	625	602	566
18.25	731	651	628	592

E Measured flapwise mode shape data for the LM17 m blade

The present appendix contains the data related to the measured flapwise mode shape of the LM17 m blade. The modulus and the phase of the complex transfer function were obtained directly from a HP3582A analyzer, which was an integrated part of the experimental setup.

In Table E.1, the measured transfer function data, taken at the excitation frequency, are listed together with the resulting (calculated) mode shape data for each of the measuring stations defined by its coordinate value.

Table E.1. Measured flapwise mode shape data.

x [m]	modulus $\|A(x,\omega_e)\|$	phase $\psi(x,\omega_e)$ [$deg.$]	mode shape $\varphi(x)$	x [m]	modulus $\|A(x,\omega_e)\|$	phase $\psi(x,\omega_e)$ [$deg.$]	mode shape $\varphi(x)$
0.00	.0	0	.00000	9.40	.132	159	.04730
0.15	.0	0	.00000	9.65	.147	159	.05268
1.00	.00261	160	.00089	9.90	.159	159	.05698
2.00	.00540	160	.00184	10.15	.170	159	.06092
2.40	.00681	160	.00232	10.40	.183	159	.06558
2.65	.00791	159	.00283	10.65	.199	159	.07131
2.90	.0093	160	.00318	10.90	.211	159	.07561
3.15	.0104	159	.00372	11.15	.225	159	.08063
3.40	.0118	160	.00403	11.40	.240	159	.08600
3.65	.0133	160	.00454	11.65	.258	159	.09245
3.90	.0154	160	.00526	11.90	.274	159	.09819
4.15	.0173	159	.00619	12.15	.292	159	.10464
4.40	.0197	159	.00705	12.40	.309	159	.11073
4.65	.0221	159	.00791	12.65	.327	159	.11718
4.90	.0250	159	.00895	12.90	.346	158	.12961
5.15	.0279	160	.00954	13.15	.365	159	.13080
5.40	.0310	159	.01110	13.40	.388	159	.13904
5.65	.0347	160	.01186	13.65	.409	159	.14657
5.90	.0387	160	.01323	13.90	.431	159	.15445
6.15	.0425	159	.01523	14.15	.457	159	.16377
6.40	.0481	160	.01645	14.40	.482	159	.17273
6.65	.0520	159	.01863	14.65	.506	159	.18133
6.90	.0574	160	.01963	14.90	.530	159	.18993
7.15	.0634	159	.02272	15.15	.560	159	.20068
7.40	.0693	159	.02483	15.40	.585	159	.20964
7.65	.0760	159	.02723	15.65	.614	159	.22003
7.90	.0829	159	.02970	15.90	.644	159	.23078
8.15	.0901	159	.03228	16.15	.675	159	.24189
8.40	.0991	159	.03551	16.40	.697	159	.24978
8.65	.107	159	.03834	16.65	.737	159	.26411
8.90	.116	159	.04157	17.00	.757	156	.30789
9.15	.125	159	.04479				

F Measured edgewise mode shape data for the LM17 m blade

The present appendix concerns the data related to the measured edgewise mode shape of the LM17 m blade. The modulus and the phase of the complex transfer function were obtained directly from a HP3582A analyzer, which were an integrated part of the experimental setup.

In Table F.1, the measured transfer function data, taken at the excitation frequency, are listed together with the resulting (calculated) mode shape data for each of the measuring stations defined by its coordinate value.

Table F.1. Measured edgewise mode shape data.

x [m]	modulus $\lvert A(x,\omega_e)\rvert$	phase $\psi(x,\omega_e)$ [$deg.$]	mode shape $\varphi(x)$	x [m]	modulus $\lvert A(x,\omega_e)\rvert$	phase $\psi(x,\omega_e)$ [$deg.$]	mode shape $\varphi(x)$
0.00	.0	0	.00000	9.40	.257	106	.24704
0.15	.00140	103	.00136	9.65	.270	106	.25954
1.15	.00773	105	.00746	9.90	.285	106	.27395
2.15	.0178	105	.01719	10.15	.298	106	.28645
2.40	.0224	106	.02153	10.40	.312	106	.29991
2.65	.0247	105	.02385	10.65	.325	107	.31079
2.90	.0296	106	.02845	10.90	.339	106	.32586
3.15	.0344	106	.03306	11.15	.353	106	.33932
3.40	.0379	106	.03643	11.40	.371	107	.35478
3.65	.0441	106	.04239	11.65	.385	106	.37008
3.90	.0487	106	.04681	11.90	.400	106	.38450
4.15	.0577	106	.05546	12.15	.413	106	.39700
4.40	.0617	106	.05930	12.40	.425	106	.40853
4.65	.0689	106	.06623	12.65	.445	107	.42555
4.90	.0746	106	.07171	12.90	.462	106	.44410
5.15	.0825	106	.07930	13.15	.470	107	.44946
5.40	.0907	106	.08718	13.40	.487	107	.46572
5.65	.102	106	.09804	13.65	.506	107	.48389
5.90	.108	106	.10381	13.90	.526	107	.50301
6.15	.117	106	.11246	14.15	.538	106	.51715
6.40	.125	106	.12015	14.40	.560	106	.53830
6.65	.135	106	.12977	14.65	.581	106	.55849
6.90	.146	106	.14034	14.90	.602	107	.57569
7.15	.152	106	.14611	15.15	.620	108	.58965
7.40	.163	106	.15668	15.40	.647	108	.61533
7.65	.174	106	.16725	15.65	.677	108	.64386
7.90	.187	106	.17975	15.90	.703	107	.67228
8.15	.196	106	.18840	16.15	.722	108	.68666
8.40	.209	106	.20090	16.40	.753	108	.71614
8.65	.219	106	.21051	16.65	.772	107	.73826
8.90	.233	106	.22397	17.00	.811	100	.79867
9.15	.244	106	.23454				

G Measured flapwise mode shape data for the LM19 m blade

The present appendix contains the measured data related to the first– and second flapwise mode shape of the LM19 m blade. The modulus and the phase of the complex transfer function were obtained directly from a HP3582A analyzer, which was an integrated part of the experimental setup.

In the Tables G.1 and G.2, the two sets measured transfer function data, taken at the excitation frequency, are listed together with the resulting (calculated) mode shape data for each of the measuring stations defined by its coordinate value.

Table G.1. Measured data related to the first flapwise mode shape.

x [m]	modulus $\lvert A(x,\omega_e)\rvert$	phase $\psi(x,\omega_e)$ [$deg.$]	mode shape $\varphi(x)$	x [m]	modulus $\lvert A(x,\omega_e)\rvert$	phase $\psi(x,\omega_e)$ [$deg.$]	mode shape $\varphi(x)$
0.00	.0	0	.00000	10.75	.170	-30	-.08500
1.00	.00197	-32	-.00104	11.00	.184	-30	-.09200
2.00	.00406	-36	-.00238	11.25	.197	-29	-.09550
3.00	.00766	-30	-.00383	11.50	.212	-30	-.10600
3.25	.00902	-31	-.00464	11.75	.228	-30	-.11400
3.50	.0102	-34	-.00570	12.00	.244	-30	-.12200
3.75	.0118	-30	-.00590	12.25	.259	-30	-.12950
4.00	.0134	-30	-.00670	12.50	.276	-29	-.13380
4.25	.0153	-30	-.00765	12.75	.295	-29	-.14301
4.50	.0174	-30	-.00870	13.00	.313	-29	-.15174
4.75	.0194	-30	-.00970	13.25	.337	-29	-.16338
5.00	.0222	-30	-.01110	13.50	.358	-29	-.17356
5.25	.0247	-30	-.01235	13.75	.379	-29	-.18374
5.50	.0275	-30	-.01375	14.00	.400	-29	-.19392
5.75	.0305	-30	-.01525	14.25	.424	-28	-.19905
6.00	.0338	-30	-.01690	14.50	.446	-29	-.21622
6.25	.0366	-30	-.01830	14.75	.469	-29	-.22737
6.50	.0405	-30	-.02025	15.00	.500	-28	-.23473
6.75	.0446	-30	-.02230	15.25	.510	-28	-.23943
7.00	.0489	-30	-.02445	15.50	.541	-27	-.24560
7.25	.0540	-30	-.02700	15.75	.569	-28	-.26712
7.50	.0590	-30	-.02950	16.00	.598	-28	-.28074
7.75	.0639	-30	-.03195	16.25	.617	-27	-.28011
8.00	.0698	-30	-.03490	16.50	.646	-28	-.30327
8.25	.0762	-30	-.03810	16.75	.689	-29	-.33403
8.50	.0829	-30	-.04145	17.00	.716	-28	-.33614
8.75	.0901	-30	-.04505	17.25	.740	-28	-.34740
9.00	.0980	-30	-.04900	17.50	.773	-28	-.36290
9.25	.106	-30	-.05300	17.75	.810	-28	-.38027
9.50	.114	-29	-.05526	18.00	.839	-28	-.39388
9.75	.124	-30	-.06200	18.25	.883	-28	-.41454
10.00	.135	-30	-.06750	18.50	.904	-28	-.42440
10.25	.146	-30	-.07300	18.75	.931	-27	-.42266
10.50	.159	-30	-.07950				

Table G.2. Measured data related to the second flapwise mode shape.

x [m]	modulus $\|A(x,\omega_e)\|$	phase $\psi(x,\omega_e)$ [$deg.$]	mode shape $\varphi(x)$	x [m]	modulus $\|A(x,\omega_e)\|$	phase $\psi(x,\omega_e)$ [$deg.$]	mode shape $\varphi(x)$
0.0	.0	0	.0	10.75	.773	60	.66943
0.115	.00317	59	.00271	11.00	.790	60	.68416
1.00	.0193	58	.01636	11.25	.799	60	.69195
2.00	.0372	59	.03188	11.50	.809	59	.69344
3.00	.0705	60	.06105	11.75	.810	60	.70148
3.25	.0801	59	.06865	12.00	.809	60	.70061
3.50	.089	60	.07707	12.25	.804	60	.69628
3.75	.100	60	.08660	12.50	.789	60	.68329
4.00	.114	60	.09872	12.75	.771	60	.66770
4.25	.128	60	.11085	13.00	.742	60	.64259
4.50	.143	60	.12384	13.25	.699	60	.60535
4.75	.158	60	.13683	13.50	.654	60	.56638
5.00	.175	60	.15155	13.75	.597	61	.52214
5.25	.194	60	.16800	14.00	.543	60	.47025
5.50	.213	60	.18446	14.25	.449	62	.39644
5.75	.233	60	.20178	14.50	.361	63	.32165
6.00	.253	60	.21910	14.75	.255	63	.22720
6.25	.274	60	.23729	15.00	.137	65	.12416
6.50	.300	58	.25441	15.25	.0115	116	.01033
6.75	.321	59	.27515	15.50	.133	-123	- .11154
7.00	.346	59	.29657	15.75	.283	-121	- .24257
7.25	.372	59	.31886	16.00	.437	-121	- .37458
7.50	.399	59	.34200	16.25	.600	-121	- .51430
7.75	.427	59	.36601	16.50	.823	-122	- .69794
8.00	.458	59	.39258	16.75	1.03	-121	- .88288
8.25	.489	60	.42348	17.00	1.20	-122	-1.0176
8.50	.519	60	.44946	17.25	1.48	-122	-1.2551
8.75	.547	60	.47371	17.50	1.72	-122	-1.4586
9.00	.580	59	.49715	17.75	1.86	-120	-1.6108
9.25	.615	60	.53260	18.00	2.23	-125	-1.8267
9.50	.643	60	.55685	18.25	2.50	-122	-2.1201
9.75	.669	60	.57937	18.50	2.69	-123	-2.2560
10.00	.696	59	.59658	18.75	3.07	-125	-2.5147
10.25	.724	60	.62700	19.00	2.98	-127	-2.3799
10.50	.749	60	.64865				

H Measured edgewise mode shape data for the LM19 m blade

The present appendix concerns the data related to the measured first edgewise mode shape of the LM19 m blade. The modulus and the phase of the complex transfer function were obtained directly from a HP3582A analyzer, which was an integrated part of the experimental setup.

In the Table H.1, the measured transfer function data taken at the excitation frequency, represented in terms of modulus and phase, are listed together with the resulting (calculated) mode shape data for each of the measuring stations defined by its coordinate value.

Table H.1. Measured data related to the first edgewise mode shape.

x [m]	modulus $\|A(x,\omega_e)\|$	phase $\psi(x,\omega_e)$ [$deg.$]	mode shape $\varphi(x)$	x [m]	modulus $\|A(x,\omega_e)\|$	phase $\psi(x,\omega_e)$ [$deg.$]	mode shape $\varphi(x)$
0.00	.0	0	.0	10.75	.0970	17	.02836
1.00	.00322	17	.00094	11.00	.101	17	.02952
2.00	.00725	17	.00211	11.25	.105	17	.03069
3.00	.0124	17	.00362	11.50	.109	17	.03186
3.25	.0137	17	.00400	11.75	.113	17	.03303
3.50	.0155	17	.00453	12.00	.118	17	.03449
3.75	.0176	19	.00572	12.25	.123	17	.03596
4.00	.0190	17	.00555	12.50	.128	17	.03742
4.25	.0212	18	.00655	12.75	.132	17	.03859
4.50	.0229	17	.00669	13.00	.137	17	.04005
4.75	.0247	17	.00722	13.25	.144	17	.04210
5.00	.0273	17	.00798	13.50	.146	17	.04268
5.25	.0291	17	.00850	13.75	.151	17	.04414
5.50	.0310	17	.00906	14.00	.157	17	.04590
5.75	.0328	17	.00958	14.25	.161	17	.04707
6.00	.0355	17	.01037	14.50	.166	17	.04853
6.25	.0376	17	.01099	14.75	.172	17	.05028
6.50	.0402	17	.01175	15.00	.176	17	.05145
6.75	.0428	17	.01251	15.25	.181	17	.05291
7.00	.0448	17	.01309	15.50	.185	17	.05408
7.25	.0480	17	.01403	15.75	.190	17	.05555
7.50	.0509	17	.01488	16.00	.196	17	.05730
7.75	.0542	17	.01584	16.25	.201	17	.05876
8.00	.0580	17	.01695	16.50	.207	17	.06052
8.25	.0610	17	.01783	16.75	.211	17	.06169
8.50	.0647	17	.01891	17.00	.217	17	.06344
8.75	.0681	17	.01991	17.25	.222	18	.06860
9.00	.0709	17	.02072	17.50	.227	17	.06636
9.25	.0747	17	.02184	17.75	.237	18	.07323
9.50	.0784	17	.02292	18.00	.246	18	.07601
9.75	.0817	17	.02388	18.25	.251	18	.07756
10.00	.0849	17	.02482	18.50	.260	18	.08034
10.25	.0890	17	.02602	18.75	.262	18	.08096
10.50	.0923	17	.02698	19.00	.324	20	.11081

Bibliographic Data Sheet **Risø–R–773(EN)**

Title and author(s)

Experimental Determination of Stiffness Distributions and Mode Shapes of Wind Turbine Blades

Gunner C. Larsen and Allan Kretz

ISBN	ISSN
87–550–2015–1	0106–2840

Dept. or group	Date
Test Station for Wind Turbines Dept. of Meteorology and Wind Energy	March 1995

Groups own reg. number(s)	Project/contract No.
0106–2840	ENS–5332/93–001

Pages	Tables	Illustrations	References
58	13	28	4

Abstract (Max. 2000 char.)

Two non–destructive experimental methods, related to the structural properties of wind turbine blades, have been formulated and applied to two different blades.

The first method deals with determination of the flexural rigidities of wind turbine blades and is based on static deflection measurements. The procedure has been applied to determine distribution of flapwise– and edgewise flexural rigidities of the LM17 m and the LM19 m blade. The findings have been compared to results obtained from cross section calculations, and the overall agreement between measured and calculated flexural rigidities is good, except for the edgewise rigidities related to the LM19 m blade, where some deviations are observed. The reason for this disagreement is believed to be a poor resolution of the curvature in the root part of the blade due to a seemingly hinge like edgewise deformation mechanism here.

The second method deals with the determination of blade mode shapes. The method is founded on an experimental determination of the transfer function relating a dynamic loading with the corresponding acceleration response in a suitable number of points along the structure. The method has succesfully been used to determine the first flapwise and edgewise natural modes of the LM17 m blade, and natural modes of the LM19 m blade related to the first flapwise–, the second flapwise–, and the first edgewise natural frequency.

Descriptors INIS/EDB

ELASTICITY; FLEXURAL STRENGTH; NONDESTRUCTIVE TESTING; OSCILLATION MODES; STRUCTURAL MODELS; TURBINE BLADES; WIND TURBINES

Available on request from:
Information Service Department, Risø National Laboratory (Afdelingen for Informationsservice, Forskningscenter Risø)
P.O. Box 49, DK–4000 Roskilde, Denmark
Phone (+45) 46 77 46 77, ext. 4004/4005 · Telex 43 116 · Fax (+45) 46 75 56 27

RISØ

Objective

The objective of Risø's research is to provide industry and society with new potential in three main areas:

- *Energy technology and energy planning*
- *Environmental aspects of energy, industrial and plant production*
- *Materials and measuring techniques for industry*

As a special obligation Risø maintains and extends the knowledge required to advise the authorities on nuclear matters.

Research Profile

Risø's research is long-term and knowledge-oriented and directed toward areas where there are recognised needs for new solutions in Danish society. The programme areas are:

- *Combustion and gasification*
- *Wind energy*
- *Energy technologies for the future*
- *Energy planning*
- *Environmental aspects of energy and industrial production*
- *Environmental aspects of plant production*
- *Nuclear safety and radiation protection*
- *Materials with new physical and chemical properties*
- *Structural materials*
- *Optical measurement techniques and information processing*

Transfer of Knowledge

The results of Risø's research are transferred to industry and authorities through:

- *Research co-operation*
- *Co-operation in R&D consortia*
- *R&D clubs and exchange of researchers*
- *Centre for Advanced Technology*
- *Patenting and licencing activities*

To the scientific world through:

- *Publication activities*
- *Co-operation in national and international networks*
- *PhD- and Post Doc. education*

Risø-R-773(EN)
ISBN 87-550-2015-1
ISSN 0106-2840

Available on request from:
Information Service Department
Risø National Laboratory
P.O. Box 49, DK-4000 Roskilde, Denmark
Phone +45 46 77 46 77, ext. 4004/4005
Telex 43116, Fax +45 46 75 56 27

Key Figures

Risø has a staff of just over 900, of which more than 300 are scientists and 80 are PhD and Post Doc. students. Risø's 1995 budget totals DKK 476m, of which 45% come from research programmes and commercial contracts, while the remainder is covered by government appropriations.